Stony Brook University

OFFICIAL COPY

The official electronic file of this thesis or dissertation is maintained by the University Libraries on behalf of The Graduate School at Stony Brook University.

© All Rights Reserved by Author.

Nanoindentation of Piezoelectric Materials

A Dissertation Presented

by

Guang Cheng

to

The Graduate School

in Partial Fulfillment of the

Requirements

for the Degree of

Doctor of Philosophy

in

Materials Science and Engineering

Stony Brook University

May 2013

Copyright by
Guang Cheng
2013

Stony Brook University

The Graduate School

Guang Cheng

We, the dissertation committee for the above candidate for the Doctor of Philosophy degree, hereby recommend acceptance of this dissertation.

Dr. T. A. Venkatesh – Dissertation Advisor

Assistant Professor, Materials Science and Engineering

Dr. Tadanori Koga- Chairperson of Defense

Associate Professor, Materials Science and Engineering

Dr. Yizhi Meng

Assistant Professor, Materials Science and Engineering

Dr. Maen Alkhader

Assistant Professor, Mechanical Engineering

This dissertation is accepted by the Graduate School

Charles Taber

Interim Dean of the Graduate School

Abstract of the Dissertation

Nanoindentation of Piezoelectric Materials

by

Guang Cheng

Doctor of Philosophy

in

Materials Science and Engineering

Stony Brook University

2013

Piezoelectric materials, with their unique electromechanical coupling characteristics, have found widespread use in many applications as sensors and actuators. With a continuing demand for macroscale piezoelectric devices with better performance characteristics, numerous efforts have been made to synthesize “bulk” monolithic and composite piezoelectric materials with better properties. More recently, within the context of microscale devices such as smart MEMS, self-powered sensors, microbatteries, and energy harvesting devices, there is a growing interest in developing “thin-film” piezoelectric materials. While, advances in microfabrication technology have greatly helped the synthesis and fabrication of piezoelectric thin films and structures, there is a continuing need to develop small-scale test methods to characterize the properties of such thin film piezoelectric materials. While nano-indentation-based methods of property determination have been demonstrated to provide useful information about the mechanical properties – elastic, plastic, hardness, and fracture properties, of metallic materials in the thin film form, comprehensive efforts to develop the nanoindentation (or indentation) technique for understanding the electromechanical properties of thin-film piezoelectric materials are not available.

The objectives of the present work are: (i) to obtain a comprehensive understanding of the indentation response of several classes of anisotropic piezoelectric materials; (ii)

to elucidate the role of the indenter geometry and the indenter conductivity on the effective indentation response of anisotropic piezoelectric materials; (iii) to characterize the effects of electric fields on the indentation response of piezoelectric materials; (iv) to compare the indentation response of piezoelectric thin films with that of piezoelectric islands; (v) to differentiate between materials that are piezoelectrically active or passive, that is, poled and unpoled, and those that are piezoelectrically strong and weak; and (vi) to identify the principal poling directions in active materials.

Three-dimensional finite element models are developed to accurately capture the force–depth and charge–depth nanoindentation response of several classes of anisotropic piezoelectric materials such as relaxor ferroelectrics for which analytical models are at present unavailable. Upon validating the finite element model for transversely isotropic materials and with experimental results, it is demonstrated that the nanoindentation response of anisotropic piezoelectric materials displays a strong dependence on the nature of the indenter geometry and relatively weak dependence on the indenter conductivity. Furthermore, by recourse to “longitudinal” and “transverse” indentations, the nanoindentation method can also be used to identify the poling directions in piezoelectric materials as well. It is also demonstrated that the indentation of piezoelectric materials which are subjected to electric fields can be used to uniquely identify the piezoelectric characteristics of thin films that exhibit in-plane poling as well.

Dedicate to My Parents and Friends

Table of Contents

List of Figures

List of Tables

Acknowledgments

I have dreamed of becoming a PhD since very young and I am so glad that this dream could come true much earlier than I expected. Without endless help and support from the people around me, I would not finish this career.

Firstly, I would like to thank my advisor, Prof. T. A. Venkatesh for giving me such a good opportunity to study on related It is my great honor and pleasure to have the opportunity to work with Prof. T. A. Venkatesh during my PHD career. This precious experience of working with him has been very beneficial to me and will have much influence on me in my future career.

I am thankful to Hongzhi Lan for his precious suggestions and help with the finite element model of ABAQUS. I also appreciate help from Qiang Zhu and Zhenzhou Peng for MATLAB codes. I sincerely thank Prof. T. Nakamura for his guidance related to executing ABAQUS codes. I would also like to thank my labmates Sumantu Iyer, Talapady Srivatsa Bhat and Ming Tian for our long and fruitful discussions on modeling and meshing. I deeply appreciate and thank Debbie Michienzi, Chandrani Roy and Lynn Allopena for their constant help with official paperwork. I would also like to thank my fellow peers Fangzhen Wu, Huanhuan Wang, Wei Nan, Mengjia Gaowei, Xue Liang, Yingjie Yu, Liudi Zhang, Naisheng Jiang, Rui Liang, Zhihua Gan and Canxing Qiu for many discussions on the subject matter.

I would like to thank my committee members Prof. T. Koga, Prof. Maen Alkhader and Prof. Yizhi Meng for their support and time. I would also like to thank Prof. Yizhi Meng, Prof. Maen Alkhader, as well as Prof. Michael Dudley for support in the application of distinguished doctoral student.

I am grateful to the Department of Materials Science and Engineering for supporting me and giving me a great platform to pursue my PhD.

I would also thank two important mentors in my life: Prof. Biao Yan in Tongji University and Mr. Sunze Dong in my high school for their mottos and help.

At last, I would special thank beloved my father, Hefang Cheng, and loving my mother, Bingqing Cao for their long time help and support in my growth and development.

Chapter 1 Background and Motivation

1.1 Piezoelectric materials

Piezoelectricity – a direct conversion of mechanical stress to the electrical charge and vice versa – has been discovered about 130 years ago. Since then, piezoelectric materials have attracted a lot of interest for application as well as fundamental research. These days, synthetic piezoelectric crystals, ceramics, polymer sheets and thin/thick films are widely applied in transducers, actuators

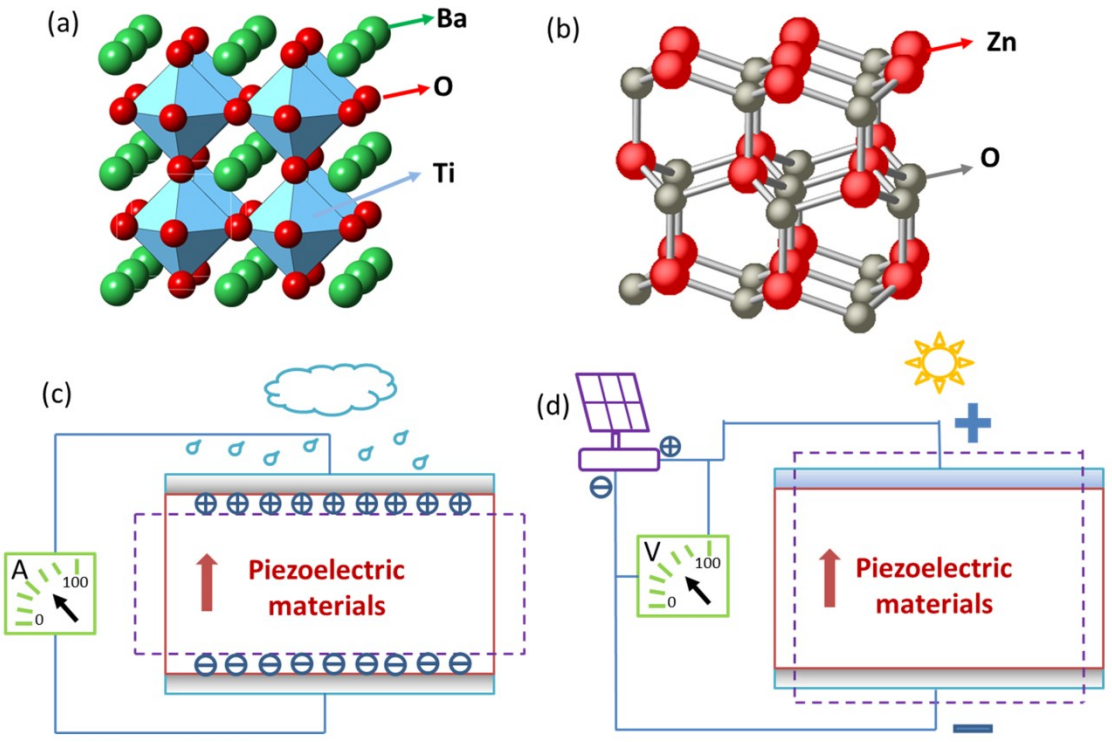

Figure 1 Schematic illustrating (a) the crystal structure of Barium Sodium Niobate ($BaTiO_3$),(b) Hexagonal wurtzites Zinc Oxide (ZnO) (c) the direct piezoelectric effect (d)the reverse piezoelectric effect

and sensors. Among these materials, Barium Titanate ($BaTiO_3$-ABO_3 type) with perovskite structure is one of most representative materials. It has been studied since 1946 as a promising material with high permittivity for ceramic capacitors. Now, it has already been easily fabricated and shaped at low price Hexagonal wurtzites Zinc Oxide (ZnO) is another example of piezoelectric/ferroelectric material and has been applied in thin films system considering their symmetry crystal structures. However, different from Barium Titanate, ZnO belongs to piezoelectric material but not ferroelectric material for its crystal structure. (Figure 1 (a) and (b)) Recently, new technologies and materials are developed to integrate piezoelectric materials in Micro Electro Mechanical Systems (MEMS) and biosensors. However, it has been difficult to access the properties of piezoelectric materials in small-volume[1, 2].

Piezoelectricity is defined as electric polarization produced by mechanical strain in crystals belonging to certain classes, the polarization being proportional to the strain and changing sign with it by Cady [3]. The direct piezoelectric effect can be identified as electric charge generated from stress and the converse piezoelectric effect can be described as mechanical movement generated from electric potential. (Figure 1 (c) and (d)) Then, based on the three basic properties (elastic modulus, piezoelectric coefficient and dielectric coefficient) of piezoelectric materials and ignoring thermal effect, the basic coupled equations for linear elastic region are shown as below

$$\sigma_{ij} = C_{ijkl}^{E}\varepsilon_{kl} - e_{ijk}E_k$$

$$D_i = e_{ikl}\varepsilon_{kl} + k_{ij}^{\varepsilon}E_j$$

Here tensor is necessary to represent mechanical and electric terms due to

solid-state as well as directional dependence of piezoelectric materials. σ_{ij} and ε_{kl} are the second rank stress and strain tensors respectively, E_k and D_i are the electric field and displacement vectors, k_{ij} is the second rank dielectric tensor, e_{ikl} is the third rank coupling tensor, and C_{ijkl} is the fourth rank elasticity tensor. Superscripts E and ε indicate that the elasticity and permittivity values are determined under conditions of zero or constant electric field and strain. Besides the signal shown above, there are also other terms and transformation relationships which might be referred in this report is listed in Table 1.

Also the above could be written as

$$\sigma_m = C_{mn}^E \varepsilon_n - e_{mn} E_n$$

$$D_m = e_{mn} \varepsilon_n + k_{mn}^{\varepsilon} E_n$$

Here m and n are transformed from ij and kl as follows: for ij or kl=11, 22, 33, 23, 13, or 12, m and n correspond to 1, 2, 3, 4, 5, or 6, respectively e.g., $\varepsilon_{12}=\varepsilon_6$ and $C_{1122}=C_{12}$. 1, 2 and 3 refer to x, y and z axis in Cartesian coordinate.

Traditionally, for bulk piezoelectric materials, small and large signal resonance methods are applied to detect the properties of piezoelectric materials by three different modes: radial mode, thickness extension mode and thickness-shear mode. For measurement of piezoelectric thin film, other than resonance methods, some contact methods, which cause direct piezoelectric effect by pneumatic pressure rig or metallic tips, were also applicable [4-6].

Table 1 Coupled constitutive relationships for linear elastic piezoelectric materials

(a)definition of various terms	
$\varepsilon_{ij} = S^{E}_{ijkl}\sigma_{kl} + d_{ijk}E_k D_i = d_{ikl}\sigma_{kl} + k^{\sigma}_{ij}E_j$ $\varepsilon_{ij} = S^{D}_{ijkl}\sigma_{kl} + g_{kij}D_k K_i = -g_{ikl}\sigma_{kl} + \beta^{\sigma}_{ij}E_j$	stress(σ) and electric field(E) are the independent variables stress(σ) and electric displacement(D) are the independent variables
E_i, D_i	electric field and electric displacement vectors, respectively
$\varepsilon_{ij}, \sigma_{ij}$	second rank strain and stress tensors ,respectively
$k^{\sigma}_{ij}, k^{\varepsilon}_{ij}$	second rank permittivity tensor where the superscript refers to the property being measured at zero or strain, respectively
$e_{ikl}, d_{ikl}, g_{ikl}$	third rank coupling tensors
S^{E}_{ijkl} , S^{D}_{ijkl}	Fourth rank compliance tensor where the superscript refers to the property being measured at zero or constant electric field or electric displacement, respectively
C^{E}_{ijkl} , C^{D}_{ijkl}	Fourth rank elasticity tensor where the superscript refers to the property being measured at zero or constant electric field or electric displacement, respectively
(b) relationship between terms in (a)	
$\beta_{ij}k_{ik} = \delta_{ik}$ $C_{ijpq}S_{pqkl} = \delta_{ijkl}$ $S^{E}_{ijkl} - S^{D}_{ijkl} = d_{mij}g_{mkl}$ $d_{nij} = e_{nkl}S^{E}_{klij}$ $k^{\sigma}_{nm} - k^{\varepsilon}_{nm} = d_{nkl}g_{mkl}$ $g_{nij} = \beta^{\sigma}_{nm}d_{mij}$ $\delta_{ij} = \begin{cases} 1, & i = j \\ 0, & i \neq j \end{cases}$	

1.2 Nanoindentation

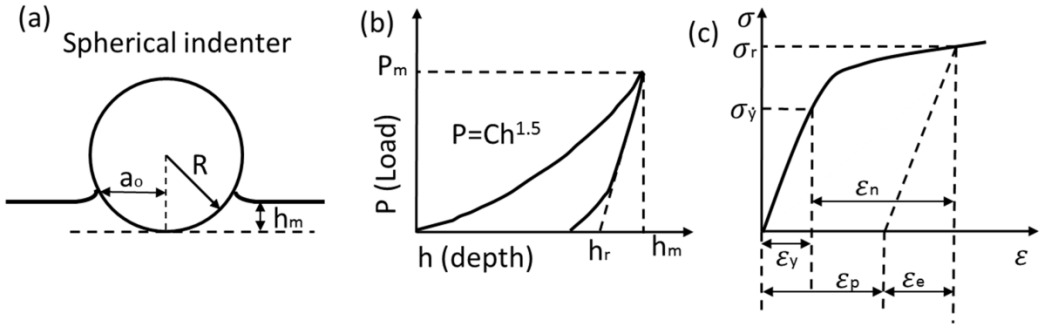

Figure 2 Schematics of: (a) spherical indentation, (b) force (P)–depth (h) indentation response f the indented material and (c) power law elasto-plastic behaviour of the indented material

In last decade, instrumental indentation has been established as a quantitative tool for the characterization of mechanical properties of materials, such as metals, alloys, ceramics, polymers, graded materials and composite material, on various scales [7-13]. Regarding the advantage of small scale and non-damage, indentation has been applied in many areas such as thin-films, coatings, and small-volume materials where conventional methods of property evaluation are not readily applicable. In previous research on indentation characterization of elastic–plastic solids, two steps of analysis, forward analysis and reverse analysis, were accomplished. In the forward analysis, the depth-indentation responses are calculated from materials properties and geometries of indenter, functional forms that relate the elastoplastic properties of the material to the principal components of the force–depth indentation response was identified. In the reverse analysis, via transforming functional forms derived from forward analysis, elasto-plastic properties are estimated from the measured indentation responses [14-19]. (Figure 2)

1.3 Prior work on nanoindentation of piezoelectric materials

In last 20 years, researchers have been trying to devise a measurement method of piezoelectric materials by instrumental nano/micro indentation. Earlier research originated from analytical models of piezoelectric contact and the first work was reported in 1987 to solve the contact problem of a circular rigid punch against a piezoelectric ceramics half-space with axial polarization. Equations of stress and electric displacement distribution on polarization direction are derived via Hankel Integral [20].

Then based on this method, analytical models of indentation on piezoelectric materials were created and modified by H. Fan, S. Suresh, A. E. Giannakopoulos, F. Q, Yang and C.Q. Chen.

Nine years later, the problem of slipping and unclipping contact on piezoelectric materials was investigated by H. Fan el at. Relationships between materials constant and stress, electric field distribution were derived under elastic deformation. Here the problem of indentation on piezoelectric materials was first solved by potential method [21].

In 1999 and 2000, a series of work about indentation of piezoelectric materials was accomplished by S. Suresh, A. E. Giannakopoulos and U. Ramamurty et al. They provided general solutions for elastic indentation of polarized transversely isotropic piezoelectric solids within elasticity were presented and optimized. Firstly, constitutive equations were deduced from conservation of linear momentum and Maxwell's electrostatic equation in cylindrical coordinate. Considering the electric properties of indenters, new

electric boundary conditions were introduced. Hankel transform/integral was employed to derive the corresponding dual integral equations for piezoelectric indentation problems that have mixed boundary conditions. Then, with factors derived from materials constants and geometry of the indenter, macroresponses (load and electric charge) and microresponses (electric potential gradient and stress distribution) could be calculated [22-24]. Later, F. Q. Yang simplified expressions for the profile of deformed surface and the distribution of electrical potential. Also, effect of electric fields on the displacement of indenter was discussed and field singularity was found when piezoelectric materials contacted with conducting indenter under a certain electric potential. Orientation problems were also considered in recent research via M. Liu and F. Q. Yang [25-28]. Almost at the same time, C.Q. Chen et al expanded the analytical models from bulk piezoelectric materials to thin film structure. The semi-empirical formulae were deduced and this relation could provide good estimates of the indentation responses for the two limiting cases of in finitely thick and thin piezoelectric films, as well as those in between [29].

Meanwhile, similar analytical solution via potential theory, a method different from Hankel integral, was also proposed by M. Kachanov and A. Makagon et al to solve constitutive equations of frictionless contact as well as equations with surface friction. Initially Corresponding Principle was developed based on potential theory to solve the contact problem of electro–elastic fields. The governing equations were derived in 3-D coordinate system and potential theory was utilized to solve conducting indenter punching on poled transversely isotropic materials. The boundary conditions applied here were the same as boundary conditions given by S. Suresh et al. Four constants were deduced from elastic tensor, piezoelectric tensor and dielectric tensor. Also with the geometry shape

and the displacement of the indenter, indentation response could be captured. These relationships helped to analyze imaging mechanisms of scanning probe microscopy on ferroelectric and piezoelectric materials. Later, frictional sliding was considered in indentation problems and the relationship was further developed to show interpretation of various scanning probe microscopy techniques of ferroelectric surfaces [30-32].

Though these two methods could deal with the piezoelectric indentation problem, a mainly difference between Hankel integral and potential theory was pointed out according to recent study: nonzero constant potential to the indenter would lead to a usual square root singularity in the induced stress field at the edge of contact [29].

Besides analytical models, some numerical methods, such as finite element analysis were also used to help people understand the process of indentation on piezoelectric materials**.**

A. E. Giannakopoulos has developed finite element models for indentation PZT-4, PZT-5A and $BaTiO_3$ with spherical indenter under zero electric potential. Micro contours of indentation stress and electric potential were displayed. Also indentation stiffness was calculated from the finite element method and comparison between finite element results and theory results are shown. Besides that, in his research, spherical indenter was recommended for testing properties of small volumes piezoelectric materials like thin films, layered plates, or composites for protecting piezoelectric surfaces [22]. Later, U. Ramamurty et al also developed finite element models for spherical indentation on transversely isotropic piezoelectric materials. From the simulation, the contours for maximum principal tensile stress and electric potentials were exhibited to show the difference between poled/unpoled piezoelectric materials and

insulating/conducting indenters [33].

Recently, E.N. Pan et al developed a new analytical model to calculate the solutions to indentation problems of multi-ferroelectric materials with axisymmetric magneto-electro-elastic property. Via half-space Green's functions, indentation responses of piezomagnetic materials could be predicted [34].

Also, several experiments were designed to seek the various characters of bulk piezoelectric materials during indenting experiments.

S. Suresh, A. E. Giannakopoulos and U. Ramamurty et al collected loading/unloading-depth curves from lead zirconate titanate (PZT-4) and barium titanate ($BaTiO_3$) under spherical indenters and compared them with analytical results. Also they investigated the difference between poled/unpoled materials as well as conducting/insulating indenters experimental and gave related conclusions. Later they began to focus on electric response under spherical and conical indenters and collected time-electric current curves. In these experiments, if the load exceeded a certain values, inelastic deformation would happen and analytical model was no longer available to describe the results [23, 35, 36].

A.Rar and V. Kalinin et al prepared nanoindentation experiments to address electromechanical coupling and pressure-induced dynamic phenomena in ferroelectric/piezoelectric materials. The harmonic movement was tested by nanoindentation when there was an electric potential on the indenter tips and back side of piezoelectric materials. A load dependence of the piezoresponse was presented in single crystal PZT-4 and polycrystal $BaTiO_3$ [37].

M.F. Wong and K. Zeng investigated nanoindentation on single crystal $Pb(Zn_{1/3}Nb_{2/3})O_3$-6%$PbTiO_3$ (PZN-6%PT) in both unpoled and poled states. They observed pile–up and local damage around the indenter at ultra-low loads. Also, force-depth curves (P-h curves) and harmonic contact stiffness were collected

and analyzed for different crystal orientations [38].

Later, U. Ramamurty et al designed spherical indentation experiments and found the indentation strength of poled PZT was higher than unpoled PZT. Also the fracture imitation was switched from Hertzian cracking to subsurface damage initiation after the polarization of materials [33].

Indentation problems on piezoelectric composites, thin films, nanowire, and nanoislands also attracted great interesting regarding their potential application in materials testing/characterization and energy harvesting.

In 1999, D.F. Bahr et al prepared 600 nm PZT thin films via solution deposited method on metallized Si wafers and testing the mechanical properties, including the hardness, modulus, and fracture behavior, of this PZT thin film system. In their research, the thin film was slightly soft than bulk PZT materials and the fine grain size, which was about 100nm, could bring in plastic deformation. Also, significant cracks generated when load of indenter was 20 mN and cracks went perpendicular to the normal to plane of the film [39].

Later, V. Koval et al also prepared similar PZT thin films system but focused on the ferroelectric behaviors of PZT thin film during indentation. Quasi-static current/charge-force hysteresis loops for thin film were presented and according to the research, the PZT thin film could fully recover with weak hysteresis. However, strong in-plane clamping stresses could cause incomplete recovery. Also, high residual stress would lead to polarization switching and domain-wall could improve the effective piezoelectric coefficient by 35% [40].

Then M.J. Reece et al gave a comprehensive research on the indentation problems of piezoelectric thin films and focused more on the mechanical responses. In the experiments, three kinds of spherical indenters (5 μm, 10 μm, and 20 μm) and six PZT multilayers films with different thickness (100 nm, 140 nm,

400 nm, 700 nm, 1500 nm, and 2000 nm), system were studied. Finite element models and analytical solutions were developed. Relationship between indentation modulus (EIS) versus contact radius/film thickness (a/t)，EIS versus depth of penetration, and EIS versus unloading were studied. Results from finite element models, analytical models and experiments showed good agreement between each other [41].

Also, mechanical response was studied via T.H. Fang et al and they switched to focus on the characterization of ZnO thin films via nanoindentation. Besides research results on the thin films properties and different sputtering powers in preparation process, the relationship between mechanical responses and loading time were studied. The Young's modulus and the hardness were slightly reduced with increased loading time and creeping time [42].

In 2008, C.Q. Chen et al had also worked on the analytical model of indentation on piezoelectric thin films. Hankel transformation was used to solve two limiting cases: infinitely thick (piezoelectric half-space) and infinitely thin piezoelectric films. Closed form solutions were given [29].

To make this method more practical, X.J. Zheng et al had built forward and inverse process to detect the properties of transverse isotropic piezoelectric thin films in film/substrate system. Both experiments and finite element method were applied to derive the dimensionless equations for forward analysis. With this method, the engineering constants of PZT thin films could be calculated from maximum indentation load, loading curve exponent and the maximum indentation depth. Then piezoelectric coefficient of the thin film could be derived [43].

Recently, W. Q. Chen et al considered the interface boundary conditions and substrate in piezoelectric multilayers structures. The substrate would influence the indentation response when indentation depth was large than 10% of first layers

thickness and the impact interface could soften the mechanical response of multilayers structures [44].

1.4 Objectives of the thesis

In spite of all research work listed above, there are still some problems restricting its further application in measurement of piezoelectric materials:

1. Most of these contact and indentation problems are created under the assumption that the indentation direction is same as polarized direction [20, 21, 24, 30, 34, 38, 43-45]. That means ongoing and past research was just focused on longitudinal indentation problems. If the polarization direction is vertical to indentation direction, the problem turns to a transversely indentation. This problem is still uncovered until now.

2. Most models were built in 2-D axisymmetric coordinate. So the piezoelectric materials, such as PZT-4 (lead zirconate titanate) and barium titanate, investigated in previous analytical models and finite element models were transversely isotropic materials or 6mm from crystal structure [24, 26, 29, 31, 45]. Other piezoelectric with more complex structure were undiscovered.

3. Different indentation results were reported in experiments for the same type of piezoelectric materials [33, 36, 38]. Also, some analytical models [29, 30] did not agree with previous finite element analysis [22] and certain experiments results [36]. These need further discussion.

4. There were flaws in both analytical model [29] and finite element model [41] for indentation on film piezoelectric materials referred above. Improper assumption and negligence of essential properties lead to large deviation between predicted results and real results.

So in this dissertation, in Chapter 2, the problems listed above are explained via finite element method. Then, in Chapter 3, as people have done before on dimensionless analysis of indentation on elastoplastic materials, the dominant factors of indentation responses are concluded from large number of simulations among relaxor ferroelectric materials. Besides indentation on bulk piezoelectric materials, simulation results for nanoindentation of piezoelectric thin films and nanoislands are shown and verified by experiment data in Chapter 4. Considering recent research on energy harvesting on piezoelectric nanowire, the contact responses between nanostructures (including nanoislands, nanowires and thin films) and spherical indenter are studied. The influences from geometry and size scales were illustrated. Meanwhile, the substrate effects on thin films and nanoislands are discussed in Chapter 4 and Chapter 5. In Chapter 6, the research will go further to illustrate the influence of electric field and the method to determine the polarization direction of piezoelectric materials. Finally, all conclusions are listed in Chapter 7 and suggestions for future research are proposed in Chapter 8.

Chapter 2 Nanoindentation of piezoelectric materials: Part I — Development of a three-dimensional finite element model

2.1 Introduction

As mentioned before, analytical modeling [21, 24, 26, 30, 34, 46], numerical modeling [22, 33, 41, 43] and experimental approaches [23, 32, 36, 37, 41, 43, 47-50] have been invoked to characterize the electromechanical indentation response of select classes of piezoelectric materials such as those that exhibit transverse isotropy. Nevertheless, the indentation response of other classes of piezoelectric materials such as those that exhibit a lower degree of crystal symmetry has not yet been fully understood. Hence, the objectives of the present work are: (i)to verify analytical models with two-dimensional and three-dimensional finite element models (ii) to obtain a comprehensive understanding of the indentation response of several classes of anisotropic piezoelectric materials; (iii) to elucidate the role of the indenter geometry and the indenter conductivity on the effective indentation response of anisotropic piezoelectric materials; and (iv) to differentiate between materials that are piezoelectrically active or passive, i.e., poled and unpoled, and those that are piezoelectrically strong and weak; and (v) to identify the principal poling directions in active materials.

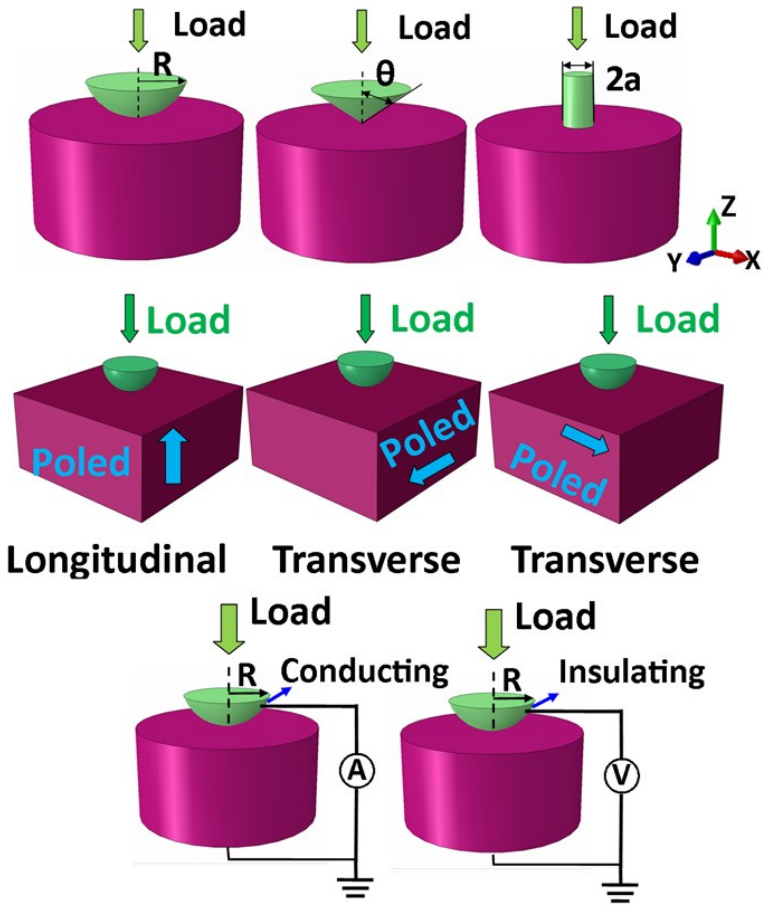

Figure 3 Schematic illustrating the indentation of anisotropic materials with conical, spherical and flat indenter using conducting or insulating indenters along the longitudinal or transverse directions.

The instrumented indentation method involves indenting a substrate material with a conical, spherical or flat indenter and measuring the complete force-depth relationship during the loading and the unloading cycle [15] (Figure 1). Within the context of piezoelectric materials, depending on the electrical boundary conditions introduced into the indentation set-up, the electric fields/voltage generated (open loop) or electric charge/current generated (closed loop) in the indentation process can be determined as well. The analytical models that have been developed for the indentation of transversely isotropic piezoelectric materials with conical,

spherical and flat conducting indenter, predict the force (P) - depth (h) and charge (Q) – depth (h) relationships as given in Table 2.

Table 2 The parameters of piezoelectric materials used in this paper (PZT is short for Lead Zirconate Titanate. BNN is short for barium sodium niobate. LN is short for lithium niobate. RL is short for relaxor ferroelectric used here)

Elastic(Gpa)					Piezoelectric(C/m^2)				
	PZT	BNN	LN	RL		PZT	BNN	LN	RL
C_{11}	121	238.9	202.9	115	e_{15}	12.3	2.763	3.424	10.1
C_{12}	75.9	104.2	52.92	103	e_{24}	12.3	3.377	3.423	10.1
C_{13}	75.4	50.06	74.91	102	e_{31}	-5.4	-0.445	0.194	-3.9
C_{22}	121	247.4	202.9	115	e_{32}	-5.4	-0.285	0.194	-3.9
C_{23}	75.4	52.14	74.91	102	e_{33}	15.8	4.335	1.309	20.3
C_{33}	111	135.1	243.1	103	e_{16}	0	0	-2.534	0
C_{44}	21.1	64.94	55.9	69	e_{21}	0	0	-2.538	0
C_{55}	21.1	65.79	55.9	69	e_{22}	0	0	2.538	0
C_{66}	22.6	75.76	74.88	66	Dielectric($10^{-10}C/Vm$)				
C_{56}	0	0	8.985	0		PZT	BNN	LN	RL
C_{14}	0	0	8.999	0	ε_{11}	81.1	20.81	7.44	127
C_{24}	0	0	-8.999	0	ε_{22}	81.1	21.87	7.44	127
					ε_{33}	73.5	26.56	2.66	60.2

In the present study, a three-dimensional finite element model is developed to simulate the indentation of anisotropic piezoelectric materials. A commercially available software package, ABAQUS, is used for developing the model. Two types of elements, C3D8E (8-node linear piezoelectric brick) type elements and C3D4E (4-node linear piezoelectric tetrahedron), are invoked. A typical model has about 208599 elements and 75113 nodes. The model is designed such that it is large enough (i.e., 20 times the contact area) to minimize end-effects and the mesh is fine enough in the indented regions for improved accuracy. Four model piezoelectric materials – Lead Zirconate Titanate (PZT-5A) [51], Relaxor

Ferroelectric (0.67 $Pb(Mg_{1/3}Nb_{2/3})O_3$ – 0.33$PbTiO_3$) [52], Barium Sodium Niobate [53], and Lithium Niobate [54] that, respectively, exhibit 6mm, 4mm, mm2, and 3m crystal symmetry are used as substrate materials for the indentation study. Parameters of these four materials were presented in Table 3. The indenter is modeled as being elastically rigid, and electrically insulating or conducting. Simulations of longitudinal and transverse indentations, i.e., indentations along the poling direction and orthogonal to poling direction of the piezoelectric materials are also conducted to understand the corresponding indentation behavior.

Table 3 Equations for indentation from analytical models [26,27]. θ = Half-apex angle of the conical indenter, R = Radius of the spherical indenter, and ao = width of the flat indenter. Constants C1 (C2 C3, C4) and C1* (C2*…. C6*) are complex functions of the elastic, dielectric and piezoelectric properties of the indented materials.

analytical [30]			
Indenter types	Load(conducting)	Charge(conducting)	Load(insulating)
Conical	$\frac{2C_1h^2tan\alpha}{\pi^2}$	$\frac{2C_2h^2tan\alpha}{\pi^2}$	N/A
Spherical	$\frac{4RC_1h}{3\pi}$	$\frac{4RC_2h}{3\pi}$	N/A
Flat	$\frac{2aC_1h}{\pi}$	$\frac{2aC_2h}{\pi}$	N/A
analytical [29]			
Indenter types	Load(conducting)	Charge(conducting)	Load(insulating)
Conical	$\frac{4C_4^*tan\theta}{\pi}h^2$	$\frac{4C_5^*tan\theta}{\pi}h^2$	$\frac{4C_1^*h^2tan\theta}{\pi}$
Spherical	$\frac{8}{3}C_4^*R^{\frac{1}{2}}h^{\frac{3}{2}}$	$\frac{8}{3}C_5^*R^{\frac{1}{2}}h^{\frac{3}{2}}$	$\frac{8}{3}C_1^*R^{\frac{1}{2}}h^{\frac{3}{2}}$
Flat	$4C_4^*a_0h$	$4C_5^*a_0h$	$4C_1^*a_0h$

2.2 Results and discussion

From the indentation study of four types of piezoelectric materials, the following principal observations are made (Figures 2-6):

1. Overall, there is good agreement between the force-depth and charge-depth relationships predicted by the analytical models [29, 30] and the finite element model developed in the present study for transversely isotropic piezoelectric materials (PZT-5A). (Figure 4)

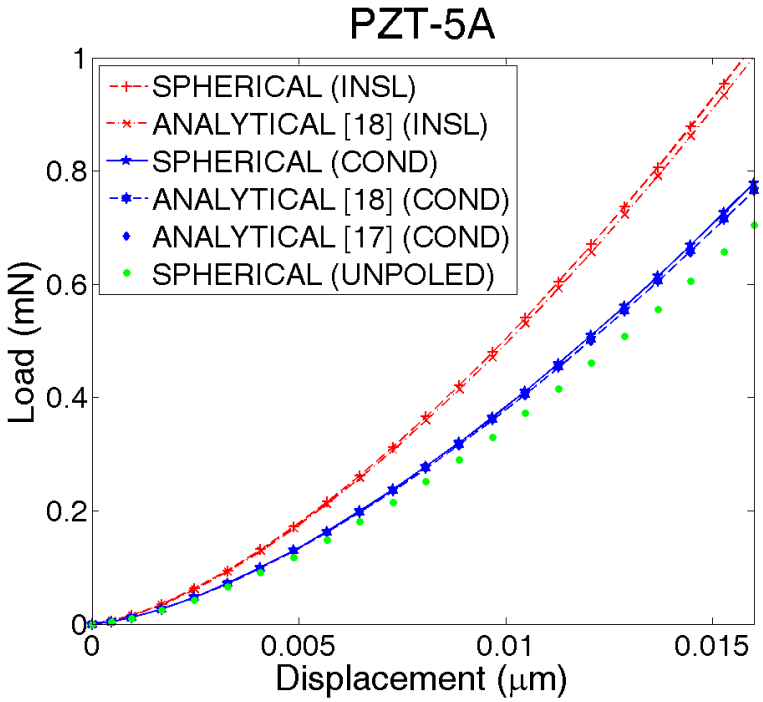

Figure 4 The force-depth indentation response obtained from the finite element analysis agrees well with the analytical model [26,27] predictions for the transversely isotropic Lead Zirconate Titanate system for spherical indentation using a conducting and insulating indenter.

2. The force-depth relationships display a strong dependence on the geometry of the indenter with the stiffest indentation response observed for indentation with

a flat indenter while the most compliant response is observed for the conical indenter in current research. (Figure 5)

3. The force-depth relationships display a weak dependence on the conductivity of the indenter (of a particular geometry) with the differences between indentations using a conducting or insulating indenter being generally small. The force-depth relationships are marginally stiffer for the indentations with an insulating indenter. (Figure 5)
4. The charge-depth relationships obtained for indentation with a conducting indenter also display a strong dependence on the indenter geometry with the maximum charges generated (at a particular depth of indentation) being obtained for indentations with a flat indenter.
5. The finite element model also captures the complete force-depth and charge-depth responses of piezoelectric materials that belong to several symmetry classes such as 4mm, mm2 and 3m for which analytical models are at present not available. It is demonstrated that the indentation response of all the materials are functionally similar in that the load-depth (i.e., P-h) and charge-depth (i.e., Q-h) relationships, respectively, follow h^1, $h^{1.5}$ and h^2 relationship for flat, spherical and conical indentations .(Table 4).
6. The indentation of the relaxor ferroelectric (with high value of e_{33} and ε_{33}) with a flat conducting indenter generates the maximum amount of charge and lithium niobate (with high value of C_{33}) with a flat indenter generates the maximum value of load for a particular depth of indentation.

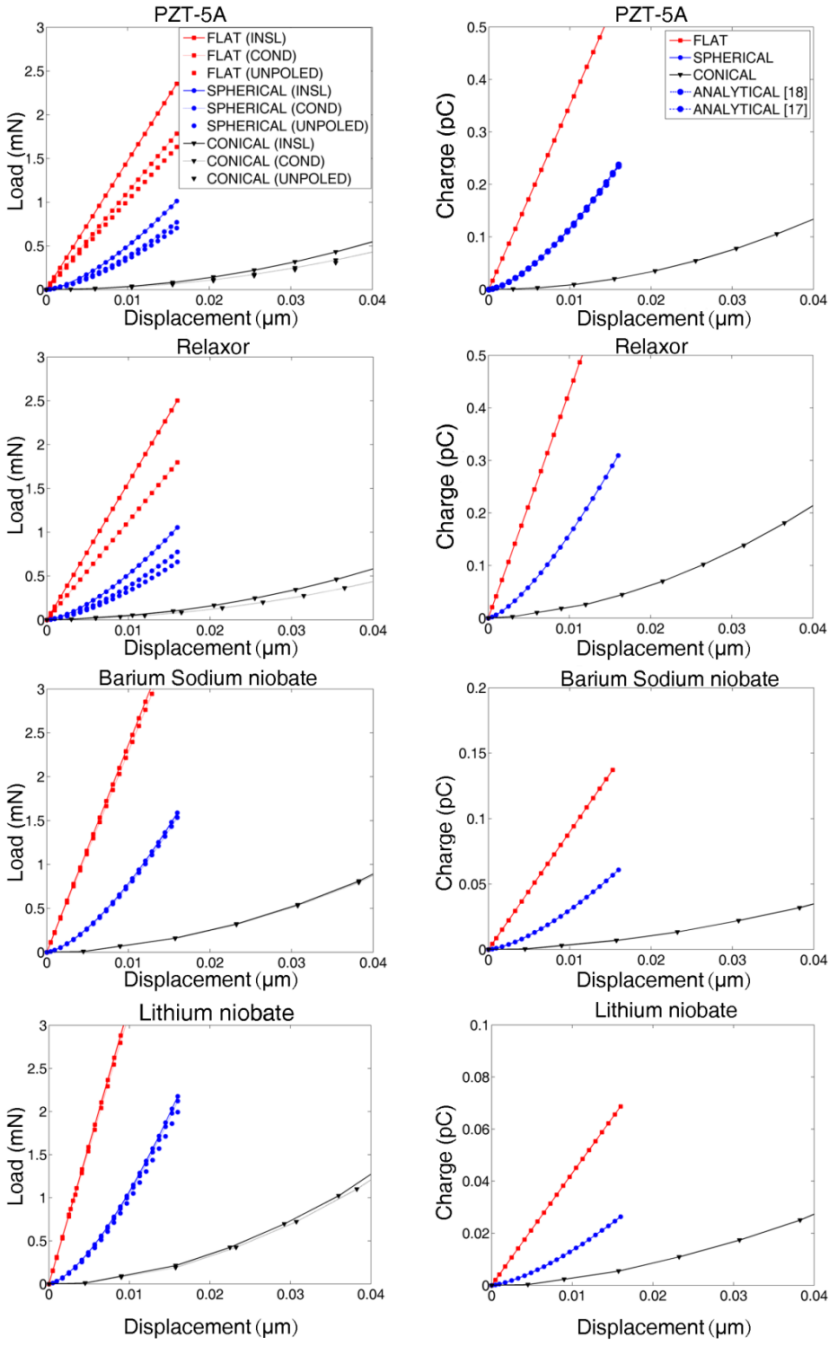

Figure 5 The force-depth and charge-depth indentation response of model piezoelectric materials – Lead Zirconate Titanate, Relaxor Ferroelectric, Barium Sodium Niobate, and Lithium Niobate, that, respectively, exhibit 6mm, 4mm, mm2, and 3m crystal symm symmetry. The charge-depth indentation response obtained from the finite element analysis agrees well with the analytical model predictions of spherical indentation [26,27] for the transversely isotropic Lead Zirconate Titanate system. (The finite element model results are presented for conical, spherical and flat indenters with $\theta=80^{\circ}$, R=15μm, and a_o = 0.75μm for conducting and insulating indenters. The indentation response of the unpoled material is also presented as well.)

Table 4 Fitting data of force-depth and charge-depth curves from indentation responses of bariums sodium niobate (BNN), lithium niobate (LN) and Relaxor ferroelectric materials (RL)

Force vs. Depth		spherical indenter $P = C_s h^{1.5}$		conical indenter $P = C_c h^2$		flat indenter $P = C_f h^1$	
		cond ($N/m^{1.5}$)	insl ($N/m^{1.5}$)	cond (N/m^2)	insl (N/m^2)	cond (N/m)	insl (N/m)
BNN	C	7.59E+11	7.84E+11	5.33E+11	5.43E+11	2.29E+11	2.36E+11
	error	1.63E+08	1.66E+08	2.95E+08	2.65E+08	3.89E+07	4.15E+07
	error/C	2.15E-04	2.12E-04	5.54E-04	4.88E-04	1.70E-04	1.75E-04
LN	C	1.05E+12	1.07E+12	7.43E+11	7.75E+11	3.15E+11	3.23E+11
	error	3.72E+08	3.30E+08	3.65E+06	3.68E+08	3.33E+07	4.37E+07
	error/C	3.56E-04	3.08E-04	4.91E-06	4.76E-04	1.06E-04	1.35E-04
RL	C	3.83E+11	5.20E+11	2.65E+11	3.58E+11	1.12E+11	1.57E+11
	error	1.02E+08	1.94E+08	3.79E+08	3.69E+08	1.47E+07	2.87E+07
	error/C	2.67E-04	3.74E-04	1.43E-03	1.03E-03	1.30E-04	1.83E-04

Charge vs. Depth		spherical indenter $Q = C_{sq} h^{1.5}$	conical indenter $Q = C_{cq} h^2$	flat indenter $Q = C_{fq} h^1$
		charge ($C/m^{1.5}$)	charge (C/m^2)	charge (C/m)
BNN	C	30.1131	1.83E+01	8.99E+00
	error	2.01E-02	1.16E-01	4.16E-03
	error/C	6.66E-04	6.32E-03	4.63E-04
LN	C	1.32E+01	1.46E+01	4.30E+00
	error	4.82E-02	7.10E-02	1.36E-03
	error/C	3.65E-03	4.86E-03	3.17E-04
RL	C	1.56E+02	1.18E+02	4.32E+01
	error	7.97E-04	8.67E-01	7.08E-03
	error/C	5.12E-06	7.36E-03	1.64E-04

7. By recognizing that there are significant differences in the force-depth and charge-depth responses of a piezoelectric material in the longitudinal and transverse indentations, the poling direction of the piezoelectric material can be identified as well. Generally, much less charge could be detected for transverse indentation than longitudinal indentation (Figure 6). Considering the transformation of properties tensor in transverse indentation, the surface charge was generated by shear stress S_{12} instead of normal stress S_{33}. So even if there was charge generated in contact region, symmetric of shear stress brought same amount of positive charges and negative charges. And these two parts cancelled each other and there would be no charge shown from macroresponses. Certain charge (1/3 of longitudinal indentation) could be observed in transverse indentation of lithium niobate. This part of charge came from transverse piezoelectric component e_{22} who become normal piezoelectric component in transverse cases.
8. Using the finite element model of indentation, the internal stress and electric field distributions can be mapped out and regions of mechanical stress and electrical field concentrations can be identified and utilized for understanding indentation-induced mechanical failures such as cracking in piezoelectric materials (Figure 7).

2.3 Conclusions

Overall, in the present study, a three-dimensional finite element model has been developed to accurately capture the indentation response of piezoelectric materials. Upon demonstrating that the finite element model predictions agree well with analytical model results for transversely isotropic piezoelectric materials,

the finite element model is extended to characterize the complete force–depth and charge–depth relationships in several anisotropic piezoelectric materials for which analytical models are at present unavailable. It is demonstrated that the nanoindentation response of anisotropic piezoelectric materials is qualitatively similar to the responses observed in transversely isotropic piezoelectric materials and displays a strong dependence on the nature of the indenter geometry and relatively weak dependence on the indenter conductivity. Furthermore, the nanoindentation method can also be used to identify the poling directions in piezoelectric materials as well.

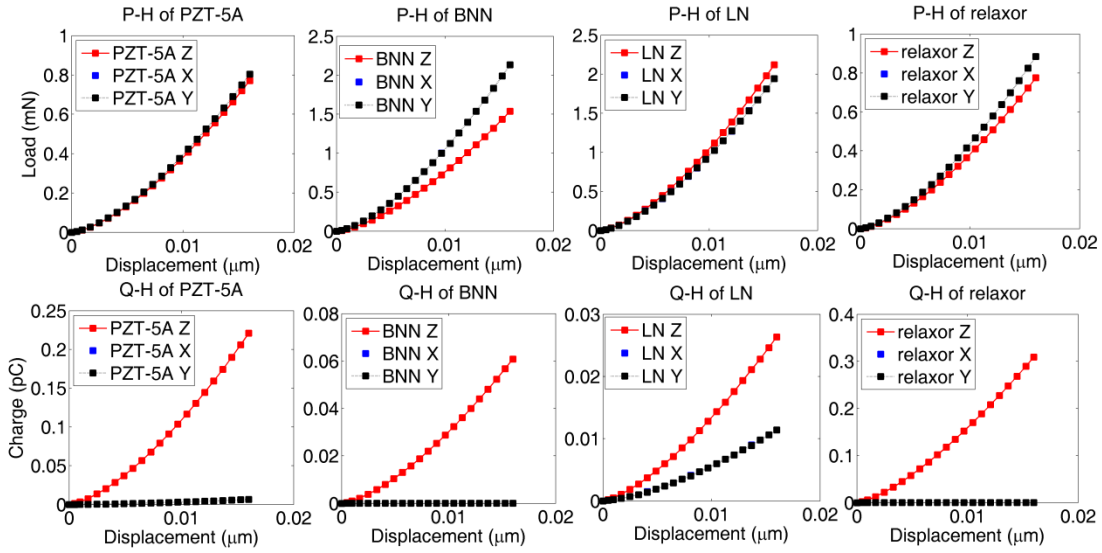

Figure 6 The force-depth and charge-depth indentation responses of four piezoelectric materials – Lead Zirconate Titanate (PZT-5A), Relaxor Ferroelectric, Barium Sodium Niobate (BNN), and Lithium Niobate obtained from 'longitudinal' and 'transverse' indentation with a conical indenter, where the indentation direction is, respectively, parallel to and orthogonal to the poling direction. (Key: Material Z indicates that the poling is along the Z direction).

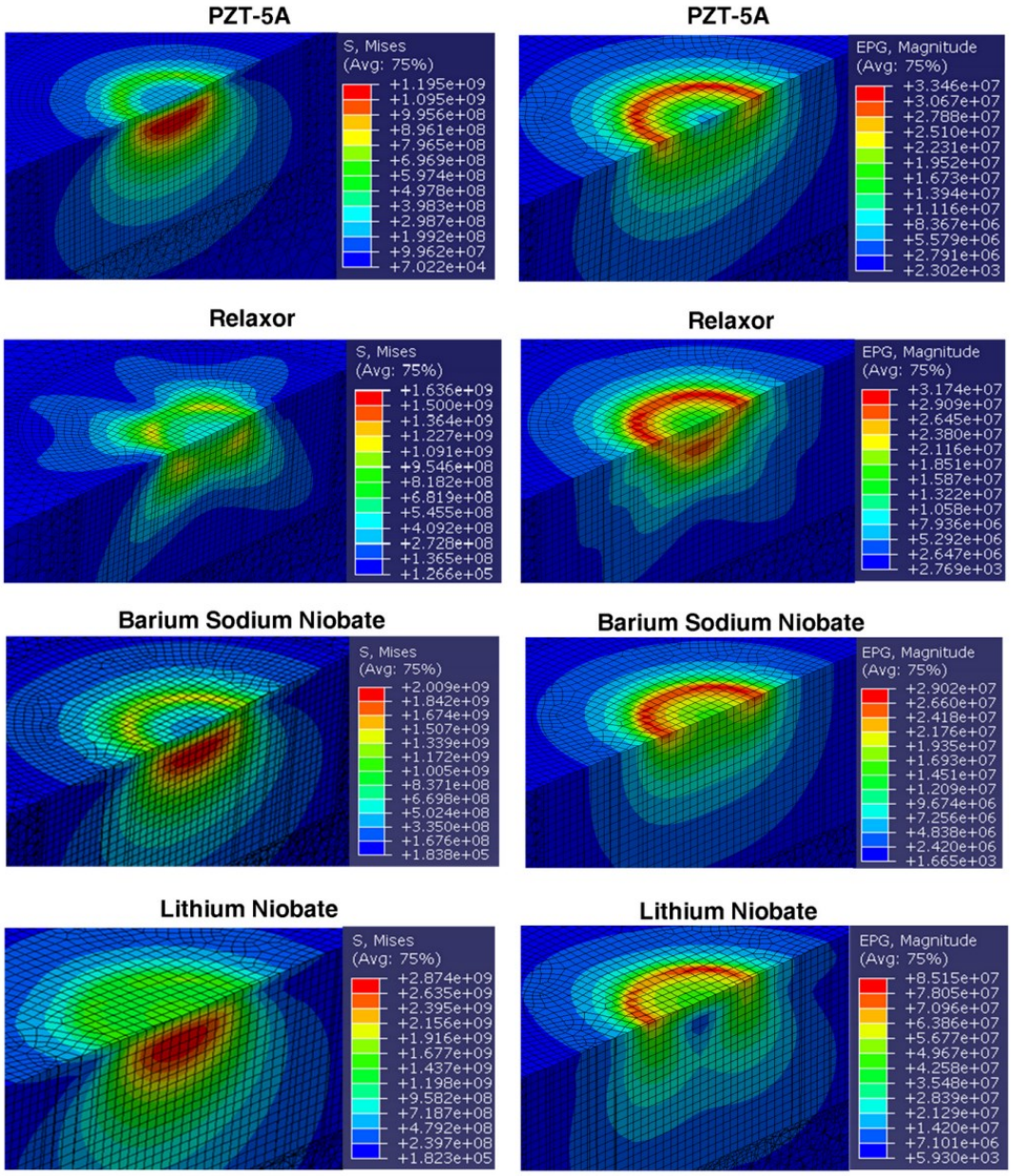

Figure 7 The maximum values of mechanical stresses (pa) and electric fields (V/m) and their spatial distributions that are obtained from the spherical indentation (with an insulating indenter) are observed to be quite different for Lead Zirconate Titanate and Relaxor Ferroelectric

Chapter 3 Nanoindentation of piezoelectric materials: Part II — Understanding the dominant factors influencing the nanoindentation response of piezoelectric materials

3.1 Introduction

The material property-indentation response relationships of piezoelectric materials as predicted by: (a) the analytical models for simple piezoelectric materials; and (b) the finite element models for more complex piezoelectric materials, it is not readily apparent as to which of the material properties have a dominant role in influencing the indentation response characteristics of simple piezoelectric materials. Hence, the objectives of the present study are:

1. to invoke existing analytical models and develop three-dimensional finite element models to obtain a comprehensive understanding of the relative importance of all the material properties in influencing the indentation response of both simple and complex piezoelectric materials;
2. to assess the relative importance of the nature of the indenter (i.e., conducting or insulating) and the indentation direction (i.e., longitudinal or transverse with respect to the poling direction of the piezoelectric material) in influencing the indentation-responses of a wide range of piezoelectric materials.

In this part, the same three-dimensional finite element model with spherical indenter was used as simulation model in chapter 3. Depending on the relative orientation of the direction of the indentation with respect to the poling direction, longitudinal and transverse indentation can be identified.

For simple piezoelectric materials in this part, PZT-5A and $BaTiO_3$ are first

chosen as model materials for a systematic investigation of the role of the individual material properties in influencing the piezoelectric response. Each of the elastic, dielectric and piezoelectric constants of PZT-5A is varied by ±10% and ±20% about its true value and the corresponding variations in the longitudinal indentation responses as predicted by the analytical model and finite element model are quantified. Furthermore, the corresponding variations in the transverse indentation responses as predicted by the finite element model are quantified as well. Following the analytical models in previous research, elastic stiffness (C_{ijkl}) instead of elastic compliance (S_{ijkl}) are used in current research to predict the variation.

Amongst the group of complex piezoelectric materials in current research, single crystal relaxor ferroelectric materials, in particular, have been recognized as promising candidates for MEMS and as actuators and transducers, owing to their strong piezoelectric properties. Consequently, many relaxor ferroelectric materials such as $Pb(Zn_{1/3}Nb_{2/3})O_3$–$PbTiO_3$ (PZN-PT), $Pb(Mg_{1/3}Nb_{2/3})O_3$-$PbTiO_3$ (PMN-PT) and $Pb(In_{1/2}Nb_{1/2})O_3$-$Pb(Mg_{1/3}Nb_{2/3})O_3$-$PbTiO_3$ (PIN-PMN-PT) single crystals which exhibit a range of chemical compositions and electromechanical properties have been synthesized [52, 55-74]. Subsequently, the indentation responses of a series of relaxor ferroelectrics are also captured using finite element simulations and the relationships between their material properties and their indentation responses are analyzed. (Table 5)

From previous research [75], depolarization effect of ferroelectric materials was mainly determined by shear stress. However, in the present study of spherical indentation of piezoelectric materials, the maximum shear stresses are typically lower than those needed for depolarization and are also confined to small

Table 5 The electromechanical properties of the piezoelectric materials that include PZT-5A, $BaTiO_3$ and several relaxor ferroelectric materials considered

Composition	Elastic (10^{10} Pa)						Piezoelectric (C/m^2)			Dielectric ($10^{-9}C/Vm$)	
	C_{11}^E	C_{12}^E	C_{13}^E	C_{33}^E	C_{44}^E	C_{66}^E	e_{31}	e_{33}	e_{15}	ε_{11}	ε_{33}
PZT-5A[51]	12.1	7.59	7.54	11.1	2.11	2.26	-5.4	15.8	12.3	8.11	7.35
$BaTiO_3$[27]	15.0	6.53	6.62	14.6	4.39	4.24	-4.32	17.5	11.4	9.87	11.2
PMN-33%PT[52]	11.5	10.3	10.2	10.3	6.9	6.6	-3.9	20.3	10.1	12.7	6.02
PMN-38%PT[72]	21.3	14.3	13.5	9.92	5.56	6.95	-3.26	11.5	21.1	19.2	2.26
PMN-28%PT[58]	15.7	14.2	11.7	10.3	7.04	1.86	-3.02	24.9	9.31	14.2	9.13
PMN-42%PT[67]	17.5	8.51	8.3	10.5	2.85	8.0	-2.1	12.2	37.5	27	2.56
PMN-0.3PTa[70]	11.7	10.3	10.1	10.8	7.1	6.6	-2.4	27.1	13.6	29.3	11
PMN-0.3PTb[62]	16.0	14.9	7.51	12.0	5.38	2.87	-5.22	31.8	30.4	43.9	12.3
PMN-35%PT[61]	14.5	15.1	7.5	11.2	3.6	3.6	-3.8	17.6	25.3	22	4.66
PZN-4.5%PT[73]	11.1	10.2	10.1	10.5	6.4	6.3	-3.7	15	8.9	26.5	8.85
PZN–7%PT[76]	11.3	10.3	10.5	10.9	6.3	7.1	-2.3	15.1	11.1	24.6	7.29
PZN–8%PT[68]	11.5	10.5	10.9	11.5	6.3	6.5	-5.1	15.4	10.1	24.1	8.71
PZN–12%PT[65]	15.2	11.4	9.7	8.72	1.9	3.6	-2.2	8.5	41.3	45.2	1.86

areas close to the region of the contact. Hence, indentation induced depolarization is not modeled in the present study. Furthermore, mechanically induced domain motions are not also considered in the present study.

3.2 Results and discussion

From the study of the nanoindentation responses of both simple and relatively more complex piezoelectric materials such as PZT-5A and relaxor ferroelectrics, the following principal observations are made:

1. There is good agreement between the predictions of the analytical model and the finite element model for the longitudinal indentation responses of simple piezoelectric materials thus validating the finite element models.(Figure 8)
2. For indentations with both conducting and insulating indenters, the mechanical indentation stiffness is influenced more by the elastic constants (such as C_{33} and C_{13}) while the electrical indentation stiffness is influenced largely by the piezoelectric constants (such as e_{33} and e_{15}) of the indented materials. The dielectric properties do not influence the mechanical indentation stiffness or the electrical indentation stiffness in a significant manner.
3. For longitudinal indentations using a conducting indenter, amongst all the elastic properties, C_{33} and C_{13}, are, respectively, the first and second most dominant material constants that influence the mechanical indentation stiffness. Similarly, amongst all the piezoelectric properties, e_{33} and e_{15} are, respectively, the first and second most dominant material constants that influence the electrical indentation stiffness. The influence of C_{33} and e_{33}, respectively, on the mechanical and electrical indentation stiffness is direct and linear. For example, a 10% or 20% increase in C_{33} results in approximately 10% or 20% increase in

the mechanical indentation stiffness. (Figure 9)

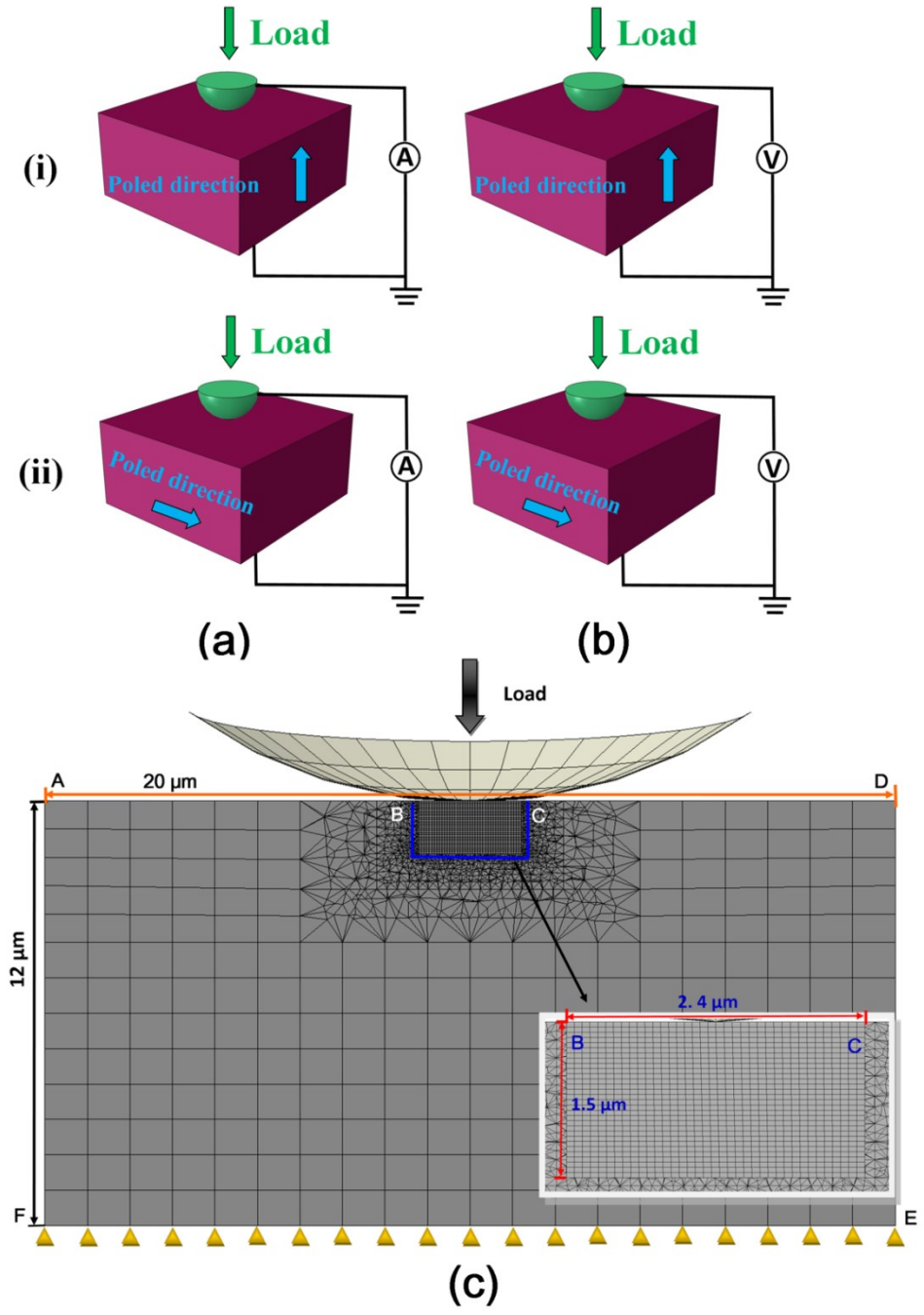

Figure 8 Schematic illustrating the indentation of piezoelectric materials with a conducting indenter (a) and insulating indenter (b) in the longitudinal direction (i) and transverse direction (ii). (c) The three-dimensional finite element model was invoked for characterizing the indentation response of piezoelectric materials.

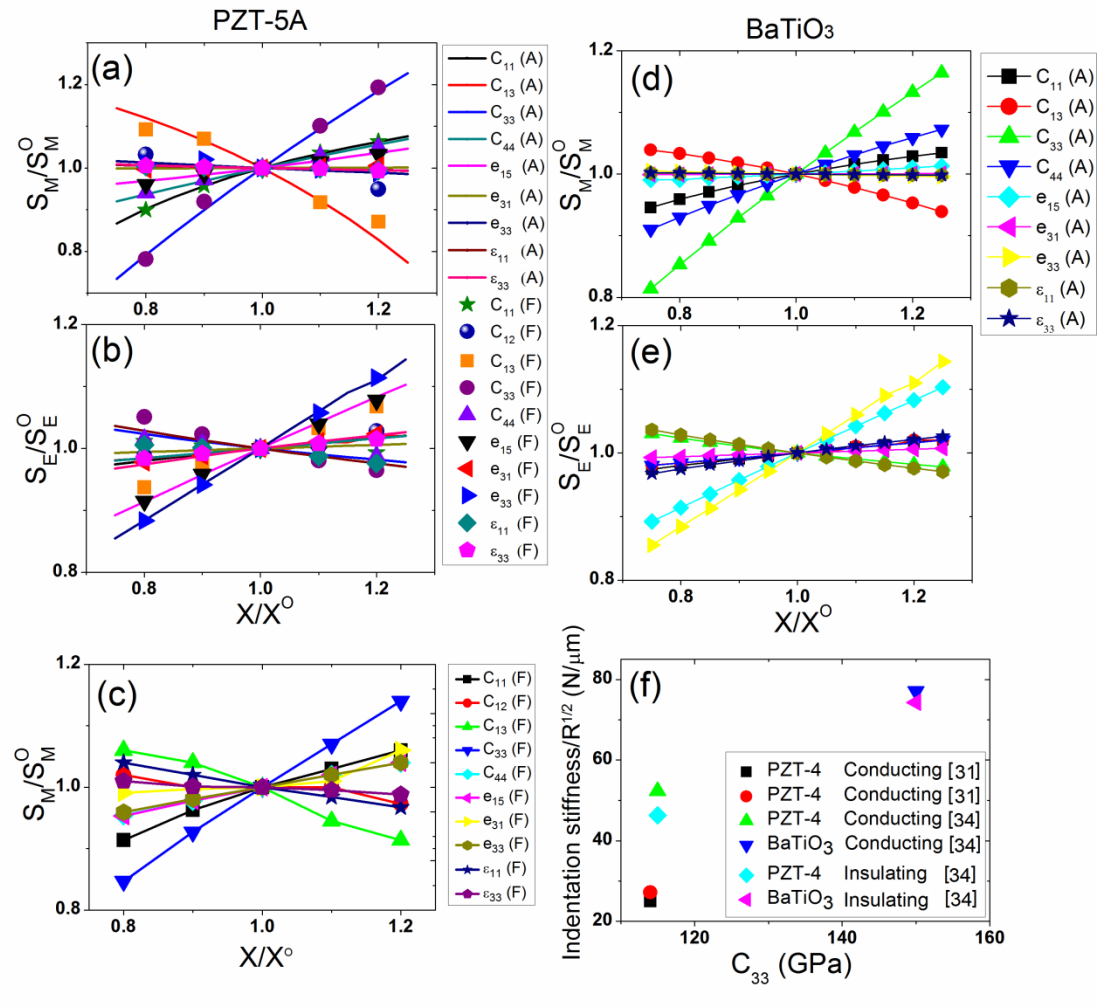

Figure 9 Normalized variations in the mechanical indentation stiffness (S_M) and the electrical indentation stiffness (S_E) for longitudinal indentations with conducting (a, b, d, e) and insulating (c) indenters observed in the analytical model [27] and finite element simulations due to variations in the individual elastic, dielectric and piezoelectric constants by ± 25% about their true values in model PZT-5A (a, b, c) and $BaTiO_3$ (d, e) piezoelectric systems. (X=material constant such as C_{33}, C_{13}, etc. A= Analytical model, F = Finite element model. For example, a + 20% change in C_{33} about its true value (i.e., C_{33}/C_{o33} = 1.2) while all other material properties are unchanged results in a 19.4% change in S_M (i.e., S_M/S_{oM}= 1.194) for indentations with a conducting indenter). (f) The experimentally observed variations of the mechanical indentation stiffness (normalized by the radius of the spherical indenter R) with the material elastic constant–C_{33}, in two materials –PZT-4 and $BaTiO_3$, for indentations with conducting and insulating indenters.

4. The experimental results on the spherical indentation of PZT-4 and $BaTiO_3$ are also observed to follow the general trend that the mechanical indentation stiffness is strongly influenced by the elasticity constant C_{33} (Figure 9 (f)). (The indentation stiffness reported by U.Ramamurty et al. [33] is lower than that reported by Ramamurty et al. [36] for PZT-4 and has been attributed to higher compliance in the experimental set-up reported in [33].)

Table 6 The variations in the effective mechanical indentation stiffness for transverse indentations with conducting (i.e., S_{mC}) and insulating (S_{MI}) indenters observed in the finite element simulations due to variations in the individual elastic, piezoelectric constants by ±10 or ±20% about their true values in a model PZT-5A piezoelectric system. (e.g., a + 20% change in C_{11} about its true value, while all other material properties are unchanged results in a 28.1% change in S_{MC})

		Elastic					Piezoelectric			Dielectric	
		C_{11}	C_{12}	C_{13}	C_{33}	C_{44}	e_{15}	e_{31}	e_{33}	ε_{11}	ε_{33}
S_{MC}	+20%	28.1	-19.7	0.76	1.35	5.22	1.17	1.61	0.55	0.83	0.89
	+10%	14.6	-8.64	0.41	0.73	3.21	1.11	1.37	0.28	0.98	1.01
	- 10%	-16.1	9.40	-0.33	-0.89	-1.32	0.97	0.91	-0.27	1.32	1.28
	- 20%	-34.8	16.7	-0.97	-2.02	-3.92	0.90	0.69	-0.55	1.51	1.43
S_{MI}	+20%	27.4	-18.6	0.41	1.21	3.74	2.59	0.82	0.24	-0.44	-0.77
	+10%	14.3	-8.26	0.24	0.65	2.29	1.66	0.43	0.13	-0.21	-0.39
	- 10%	-15.9	8.38	-0.22	-0.76	-0.93	-0.17	-0.36	-0.16	0.29	0.50
	- 20%	-34.7	14.9	-0.66	-1.66	-2.73	-1.05	-0.74	-0.35	0.57	1.45

5. For transverse indentations using a conducting indenter, C_{11} and C_{12} are, respectively, the first and second most dominant material constants that influence the mechanical indentation stiffness. However, the influence of C_{11} and C_{12} on the mechanical stiffness is about 50% greater than that observed in the case of longitudinal indentations. (Table 6)

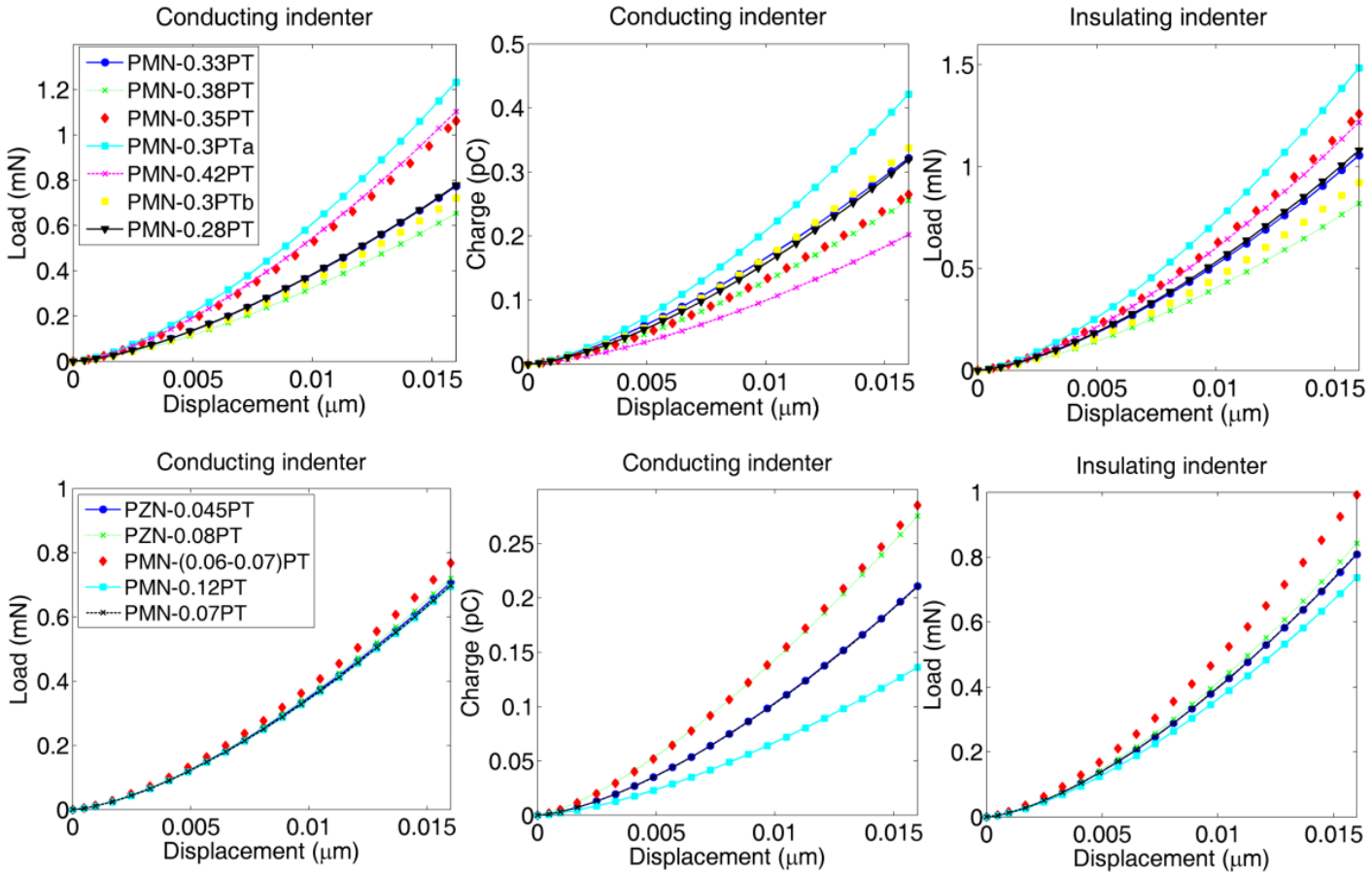

Figure 10 Force-depth (P-H) and charge–depth (Q-H) nanoindentation responses obtained from the indentation of relaxor ferroelectrics PMN-xPT and PZN-xPT using conducting and insulating spherical indenters.

6. For longitudinal indentations using an insulating indenter, the influence of the mechanical constant C_{33} on the mechanical indentation stiffness is lower than that observed in the case of indentations with a conducting indenter.

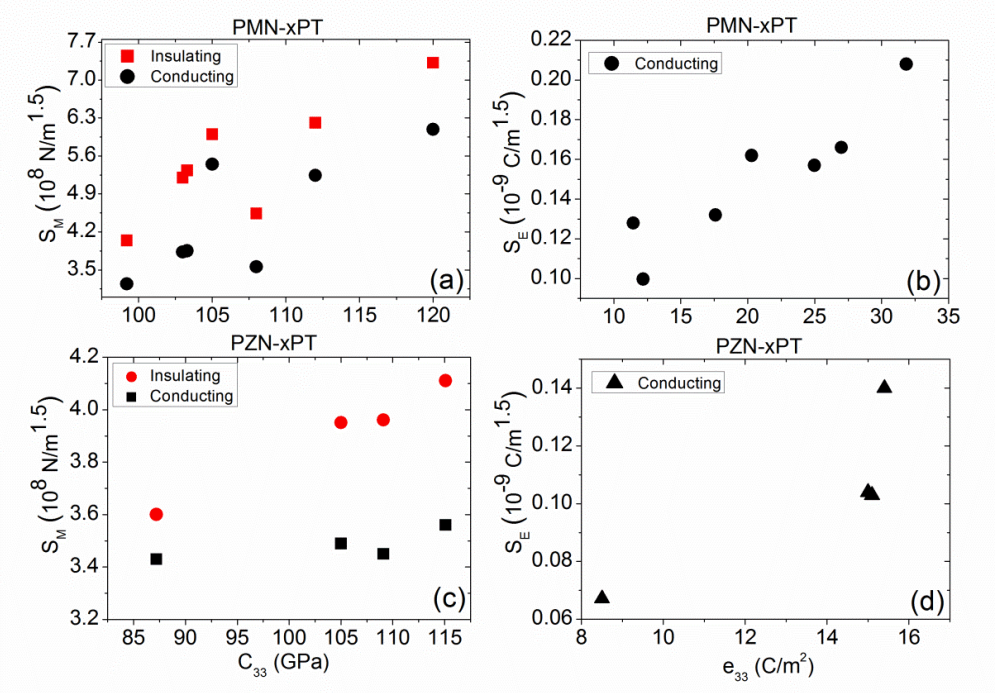

Figure 11 Variations in the mechanical indentation stiffness (S_M) (for indentations with conducting and insulating indenters) and the electric indentation stiffness (S_E) (for indentations with a conducting indenter) with, respectively, the elastic constant (C_{33}) and the piezoelectric component (e_{33}) in a series of relaxor ferroelectrics – PMN-xPT (a and b) and PZN-xPT (c and d).

7. In analyzing the indentation responses of relaxor ferroelectrics based on PMN-xPT and PZN-xPT which exhibit a range of elastic, dielectric and piezoelectric properties, it is generally observed that materials with higher normal elastic and piezoelectric properties, i.e., C_{33} and e_{33}, (Figure 10 and Figure 11). Similarly, the relationship between the inverse of the compliance constant S_{33} (i.e., $1/S_{33}$) and the mechanical indentation stiffness was also found to be direct and linear as well. Furthermore, for those materials that exhibited similar e_{33} properties, their electrical indentation stiffness is

influenced by e_{15} as well (Figure 11).

8. In the indentation of relaxor ferroelectrics, it is observed that the (mechanical or electrical) indentation stiffness does not increase monotonically with an increase in the material constant, C_{33} or e_{33} (e.g., Figure 11**a**). This observation can be explained as follows. Figure 11a captures the variation of the indentation stiffness as a function of only one mechanical constant (e.g., C_{33}) in a series of relaxor ferroelectrics (where each material has a unique combination of 11 material constants). The influence of other material constants such as C_{13}, C_{44} or e_{15} which also influence the indentation stiffness is not captured explicitly in Figure 11**a**. For example, two relaxor ferroelectrics have two combinations of the material constants C_{33} and C_{13} PMN-42%PT (C_{33} = 105 Gpa and C_{13} = 83 Gpa) and PMN-0.3PT (C_{33} = 108 Gpa and C_{13} = 101 Gpa). As presented in Figure 9, an increase in the C_{33} constant increases the indentation stiffness while an increase in the C_{13} constant decreases the indentation stiffness. Thus, PMN-0.3PT, which has a marginally higher C_{33} (as compared to that of PMN-42%PT), exhibits lower indentation stiffness when compared to that of PMN-42%PT because the C_{13} constant of PMN-0.3PT is much higher than that of PMN-42%PT.
9. In the indentations of relaxor ferroelectrics, for those materials that exhibit higher piezoelectric constants (i.e., e33), there is a greater difference in the mechanical indentation stiffness observed for indentations with conducting and insulating indenters.

3.3 Conclusions

Nanoindentation-based techniques, owing to their ease of experimentation

and versatility in probing the properties of materials over small-volumes, have been increasing invoked for characterizing the electromechanical properties of piezoelectric materials. However, the relationships between the elastic, dielectric and piezoelectric properties of the piezoelectric materials and their indentation responses tend to be quite complex. Hence, the present study was focused on obtaining a comprehensive understanding of the dominant factors influencing the force-depth mechanical indentation response and the charge-depth electrical indentation response of the piezoelectric materials. By invoking an analytical model developed earlier for predicting the indentation response of relatively simple piezoelectric materials (such as PZT-5A) and a large number of three-dimensional finite element simulations for characterizing the indentation response of simple and complex piezoelectric materials (such as relaxor ferroelectrics), the following principal conclusions were obtained:

1. For indentations with both conducting and insulating indenters, the mechanical indentation stiffness is influenced more by the elastic properties, while the electrical indentation stiffness is influenced largely by the piezoelectric properties of the indented materials. The dielectric properties do not influence the mechanical indentation stiffness or the electrical indentation stiffness in a significant manner.
2. For longitudinal indentations using a conducting indenter, amongst all the elastic properties, C_{33} and C_{13}, are, respectively, the first and second most dominant material constants that influence the mechanical indentation stiffness. Similarly, amongst all the piezoelectric properties, e_{33} and e_{15} are, respectively, the first and second most dominant material constants that influence the electrical indentation stiffness. The influence of C_{33} and e_{33}, respectively, on the mechanical and electrical indentation stiffness is direct

and linear. For example, a 10% or 20% increase in C_{33} results in approximately 10% or 20% increase in the mechanical indentation stiffness.

3. For transverse indentations using a conducting indenter, C_{11} and C_{12} are, respectively, the first and second most dominant material constants that influence the mechanical indentation stiffness. However, the influence of C_{11} and C_{12} on the mechanical stiffness is about 50% greater than that observed in the case of longitudinal indentations.
4. For longitudinal indentations using an insulating indenter, the influence of the mechanical constant C_{33} on the mechanical indentation stiffness is lower than that observed in the case of indentations with a conducting indenter.
5. In the indentation of relaxor ferroelectrics based on PMN-xPT and PZN-xPT which exhibit a range of elastic, dielectric and piezoelectric properties, it is generally observed that materials with higher normal elastic and piezoelectric properties, i.e., C_{33} and e_{33}, respectively, exhibited higher mechanical and electrical indentation stiffnesses.
6. In the indentations of relaxor ferroelectrics, for those materials that exhibit higher piezoelectric constants (i.e., e_{33}), there is a greater difference in the mechanical indentation stiffness observed for indentations with conducting and insulating indenters.

Chapter 4 Nanoindentation of piezoelectric materials: Part III — Verification of finite element model with experiments

4.1 Introduction

Attributed to nanomechanical and electromechanical properties of piezoelectric materials in bulk, thin film and nanowire form, they are increasingly studied in energy harvesting applications to collect energy in the form of pressure transitions and vibrations. High efficient piezoelectric thin films, which could convert small mechanical vibration to voltage on the scale of silicon transistor logic, greatly help energy harvesting in microelectromechanical systems. Nanowire made from ZnO and $BaTiO_3$ have exhibited a significant advance in microscale piezoelectric energy scavenging, based on a combination of semiconductor and piezoelectric properties [77-88].

Research has been done on the adoption of thin film technology for lead zirconate titanate compounds with strontium (Sr). The addition of Sr to PZT compounds to realize strontium-doped PZT (PSZT) enhances piezoelectric and ferroelectric properties of the compound in both bulk and thin film structures. According to related research results, the normal (longitudinal) piezoelectric component d_{33} as high of 892 pm/V on gold-coated silicon and 1450 pm/V on platinum-coated silicon are reported for the piezoelectric response of $(Pb_{0.92}Sr_{0.08})(Zr_{0.65}Ti_{0.35})O_3$ compounds under the converse piezoelectric effect [89-93].

In this part, experimental data for indentation on PSZT thin film (700nm and 1400nm) and PSZT nanoislands were collected from our cooperators. Two-dimensional axisymmetric models and three-dimensional models were developed to characterize the influence of the electromechanical properties on the effective nanoindentation response of PSZT thin films and nanoislands.

4.2 Experimental procedure & FE simulation

The PSZT thin films are deposited by Radio Frequency (RF) Magnetron Sputtering, on to pre-cleaned platinum-coated silicon substrates. A 200 nm platinum coating with a 20 nm titanium dioxide (TiO_2) adhesion layer is used to form the conductive bottom electrode metallization of the silicon substrates. The PSZT thin films are deposited at a speed of 350 nm/hour to attain thicknesses of 700 nm and 1400 nm. Piezoelectric nanoislands are prepared from deposited PSZT film, of which thickness is larger than 200 nm thick and followed by lift-off with chlorobenzene. The geometry of island would be hemispherical or cylindrical, depending on the aspect ratio of the island. In the indentation test, islands with diameter of 200 and 400 nm were chosen. In the experimental test, Hysitron triboindenter is used and the corresponding force-depth curves are recorded for a range of forces from 0.1 to 10.0 mN [89-93].

For the simulation of thin films, modified two-dimensional axisymmetric models are developed to simulate the indentation response of PSZT thin films with thicknesses of 700 nm and 1400nm. The bottom side of the sample is constrained from any vertical displacement and the left side (which is actually the center of the specimen) from any horizontal displacement. The top side and the right side are not constrained mechanically. No electric boundary conditions are

applied so the indenter is in an open-circuit. Substrate dimensions are chosen to match with experimental specimens.

Table 7 Properties of doped PZT-5A to characterize their indentation response

materials	Elastic (10^{10} Pa)						Piezoelectric (pm/V)			Dielectric (10^{-9}C/Vm)	
	C_{11}^E	C_{12}^E	C_{13}^E	C_{33}^E	C_{44}^E	C_{66}^E	d_{31}	d_{33}	d_{15}	ε_{11}	ε_{33}
PZT-5A(d_{33}=374 pV/m)	12.1	7.59	7.54	11.1	2.11	2.26	-171	374	583	8.11	7.35
PZT-5A(d_{33}=1000 pV/m)	15.0	6.53	6.62	14.6	4.39	4.24	-300	1000	583	9.87	11.2

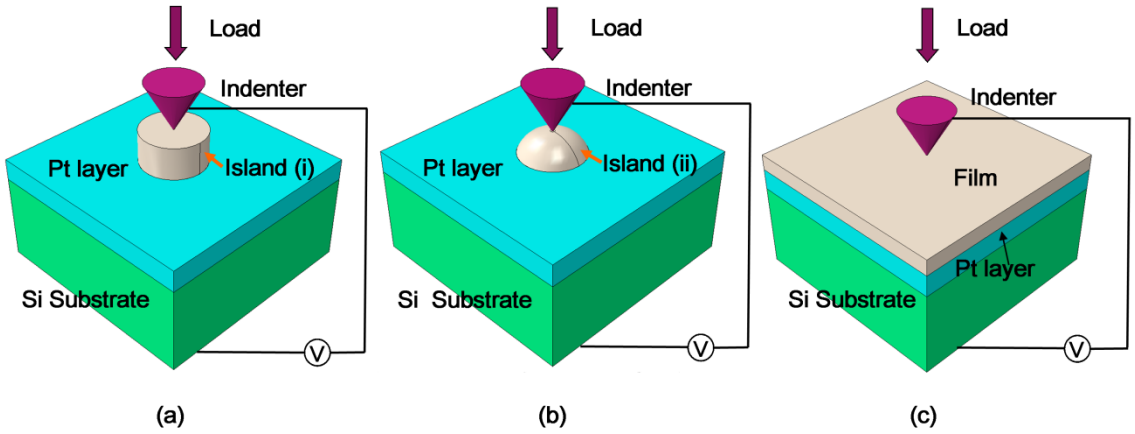

Figure 12 Schematic illustrating the indentation of piezoelectric materials with Hysitron triboindenter: (a) nanoislands (cylinder), (b) nanoislands (hemispherical) and (c) thin film

A commercially available software package, ABAQUS, is used for developing the model. For the 700 nm film, the finite element model has about 23,464 nodes comprising of 23,315 elements, which includes 6337 four-node axisymmetric (CAX4E) elements and 16,978 four-node bilinear, reduced integration axisymmetric (CAX4R) elements. For the 1400 nm film, the model has about 21,978 nodes with 21,810 elements, which includes 11,972 CAX4E and 9838

CAX4R elements. The model is designed such that it is large enough to minimize end-effects and the mesh is fine enough in the indented regions for improved accuracy. For the simulation of nanoislands, considering possible geometry of hemispherical or cylindrical, two kinds of three-dimensional FE models were designed and meshed. With the same mechanical and electrical boundary conditions for thin films indentation, the models have around 20,000 8-node linear piezoelectric brick (C3D8E) elements and 200,000 8-node linear brick, reduced integration (C3D8R) elements. Here, the Hysitron Triboindenter is simulated as equivalent Berkovich indenter with a spherical tip (R=150 nm). The materials properties are exhibited in Table 7 and the sketch of the indentation experiments is presented in Figure 12.

4.3 Results and discussion

1. There is good agreement between the results of the finite element model and the experimental results for PSZT thin film, both 700nm and 1400nm, with indentation depth no more than 7% of film thickness. From simulations, the mechanical indentation stiffness could significantly increase with high d_{33} values and it demonstrated that the doping could help PSZT thin become stiffer. Considering that the elastic modulus of Si (185 Gpa) substrate is much higher than the normal elastic component of PSZT (C_{33}=111 Gpa), the PSZT thin film structure is stiffer than bulk PSZT materials. For indentation of 700nm PSZT film, the experimental results display higher stiffness than simulation results. This would attribute to loading velocity: current simulation provides general static solutions so the influence of loading velocity is ignored. Also for the

700nm PSZT thin film, there is a significant inflection point appeared in the force-depth curves and this attributed to substrate effects. However, there is not such inflection in the force-depth curves of 1400nm PSZT thin film and the simulation results show good agreement with experimental results. (Figure 13)

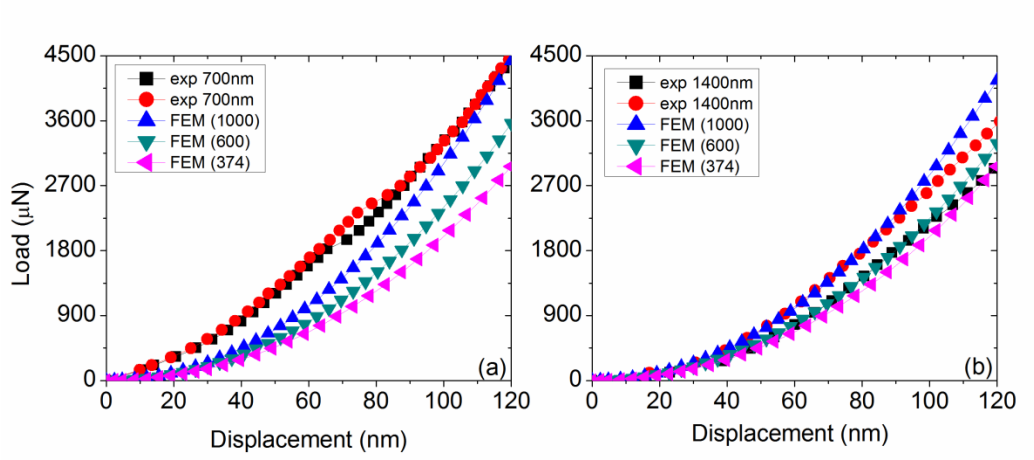

Figure 13 Force-depth response obtained from the nanoindentation of doped PZT-5A films and finite element simulations of a standard PZT-5A thin film, FEM(374), and PZT-5A thin films with enhanced d_{33} properties (d_{33}=1000 pV/m in FEM(1000) and d_{33}=600 pV/m in FEM(600), here d_{31} was assumed as 0.3 d_{33}). Results are shown for film thickness of (a) 700nm and(b)1400nm

2. Also, there is a good agreement between the results from hemispherical or cylindrical finite element models and experimental results for PSZT nanoislands in shallow indentation when indentation depth is no more than 5% of island thickness (around 10 nm). Meanwhile, compared to experimental data of 700 PSZT thin films, both simulation results and experimental data could demonstrate that nanoislands have lower indentation stiffness than films. (Figure 14)

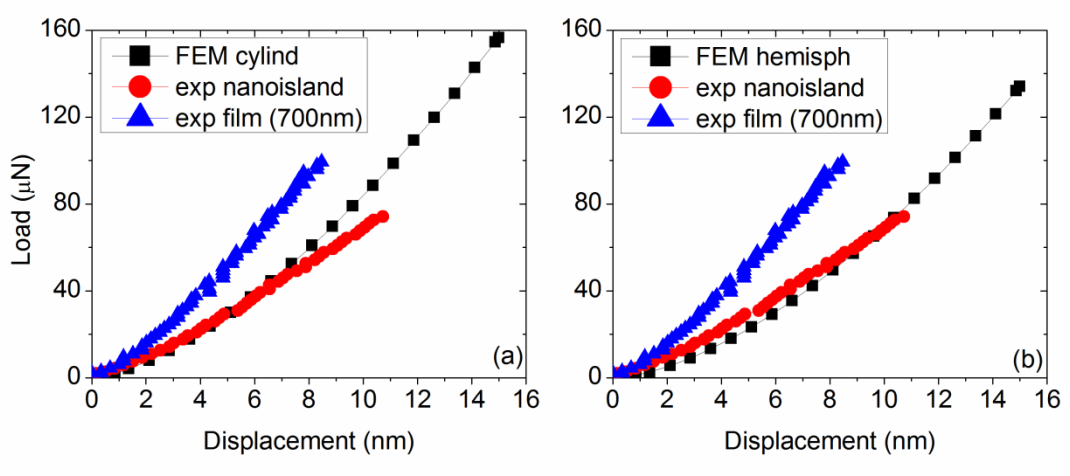

Figure 14 Force-depth response obtained from the shallow nanoindentation (indentation depth is less than 10 nm) of doped 700nm PSZT films and nanoislands compared to results from finite element simulations of (a) nanoislands (d_{33}=1000 pV/m) with cylinder structure (FEM cylind) and (b) nanoislands (d_{33}=1000 pV/m) with hemispherical structure (FEM hemisph)

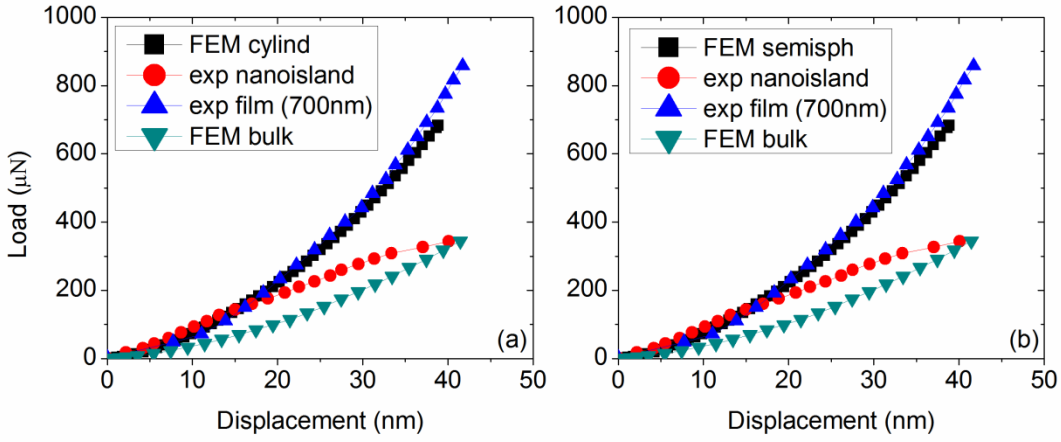

Figure 15 Force-depth response obtained from the deep nanoindentation (indentation depth is around 40 nm) of doped 700nm PSZT films and nanoislands compared to results from finite element simulations of (a) nanoislands (d_{33}=1000 pV/m) with cylinder structure (FEM cylind) and (b) nanoislands (d_{33}=1000 pV/m) with hemispherical structure (FEM hemisph). Bulk FEM from nanoindentation response of bulk unpoled PZT-5A materials

3. In deep indentation of nanoislands, when indentation load is less than 0.2mN or indentation depth is less than 20 nm, there is still good agreement between finite element models and experiment for nanoislands. Also the force-depth curves are close to each other for thin film and nanoislands within this range. Then a bifurcation is observed in experiments: the film becomes stiffer and keeps the trend; while, the nanoislands reach a maximum position and became flat. Different from bifurcation in experimental, simulation results show that force-depth curves are similar for in two kinds of island as well as thin films. Compared to bulk PZT-5A, PSZT nanoislands have higher piezoresponse and indentation stiffness (Figure 15). There might be three reasons for the bifurcation between thin film and nanoislands: (i) Contact area: with deeper indentation, the thin film could provide more contact area however nanoislands cannot. (ii) Substrate effect: nanoislands have only 200nm along indentation direction and the indentation depth had reached 20% of the thickness, however, thin film has 700nm and indentation depth was only 5% of the thickness. There is a significant stress concentration on the interface of PSZT nanoislands and platinum (Pt) layer but not on the interface of thin film and Pt layer. (iii) Possibly plastic deformation: the plastic deformation possibly originates from slip dislocations in the highly nano-columnar structures [40, 94].
4. To illustrate the substrate effects in the indentation response of PSZT thin films and nanoislands, the materials properties are modified for simulation in current models. Two kinds of properties for Pt are brought in: one is normal bulk Pt with yield stress around 260 Mpa; another is Pt with nano structures with yield stress as high as 3 Gpa [95]. Then, new indentation responses with elastoplastic properties were presented in Figure 16. From finite element

simulation and experiments, the new substrate has little influence on 700nm and 1400nm thin films when the indentation depth is limited to 10% of the thickness. As the indenter goes deeper, the plasticity of substrate begins to influence the indentation response. This phoneme is significantly observed in 700nm PSZT thin films. For the nanoislands, it is observed that the experimental curves are between the data from finite element models with nano structures Pt and normal Pt for deep indentation. Therefore, the plasticity of substrate would greatly influence the mechanical responses in deep indentation of both thin film and nanoislands.

5. From simulations results, it indicates that the geometry of nanoislands prepared in experiments is more close to cylinder than hemisphere. The cylindrical nanoislands would be much stiffer than hemispherical structure at deep indentation. (Figure 15 and Figure 16)
6. The geometry of triboindenter indenter has significant influences on the indentation responses. From the fitting data of simulation results, the force-depth curves could fit the power law $P=Ch^{1.5}$ at shallow indentation and turn to $P=Ch^{2}$ for deep indentation.
7. Based on these results, the indentation response of thin film and nanoislands with Pt and silicon substrate could be divided into three steps: step (i), within indentation depth less than 10% piezoelectric structures, only elastic deformation are observed in piezoelectric structures and substrate; step (ii), within indentation depth between 10% and 20% piezoelectric structures, elastic deformation of piezoelectric structures and plastic deformation of substrate are found; step (iii), within indentation depth large than 20%, plastic deformation or breakdown (fracture) of piezoelectric structures as well as plastic deformation of substrate might happen

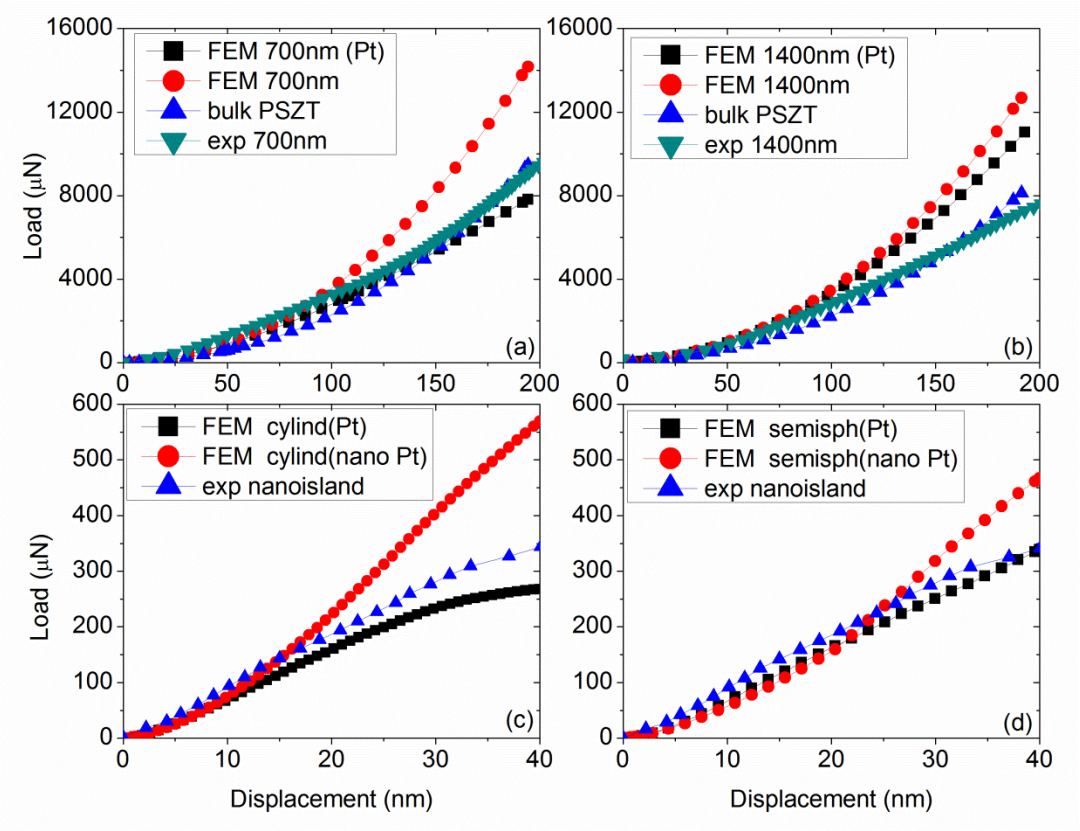

Figure 16 Force-depth response obtained from the nanoindentation of doped 700nm PSZT films and nanoislands compared to results from finite element simulations considering elastoplastic properties (Pt refers ordinary bulk platinum with yield stress at 265Mpa and and 0 hardening nano Pt refers plastic properties of nanostructured Pt [96]) of Pt layer in substrate: (a) 1400nm thin film (d_{33}=1000 pV/m), (b) 700nm thin film (d_{33}=1000 pV/m), (c) nanoislands (d_{33}=1000 pV/m) with cylinder structure and (d) nanoislands (d_{33}=1000 pV/m) with hemispherical structure

4.4 Conclusions

Overall, finite element method is successfully verified via the experimental results for the nanoindentation problems on doped PZT-thin films and nanoislands. From the simulation results, the doped effect could render the PZT-5A film stiffer than bulk materials. Also the finite element models could accurate capture the indentation response of nanoislands considering influences from both geometry

as well as substrate effects. Finally based on the simulation and experimental results, the process of indentation on piezoelectric thin films and nanoislands was summarized as three steps.

Chapter 5 Nanoindentation of piezoelectric materials: Part IV — Understanding the effects of geometry: implications for piezoelectric nanoislands, nanowires and thin films

5.1 Introduction

To prolong the lifespan of portable wireless devices, it is a good choice to design energy scavenging devices which could covert possible energy to electric energy. In recent research, several piezoelectric nanostructures, including nanoislands, nanofibers, nanowire and thin films have been designed and made from zinc oxide (ZnO), lead zirconate titanate (PZT), gallium nitride and barium titanate. These nanostructures could serve as nanogenerators via converting low-frequency vibrate mechanical energy into electric potential with small movement of metal coated cantilever. Z.L. Wang et al had developed several energy harvesting devices via nanowire/nanofibers via ZnO on plastic/fibers and these devices could collect energy on low frequencies (<10Hz) and the electrical voltage could reach 6 V [77, 81, 82, 85, 87]. Then, Xi Chen et al designed PZT nanofibers generators with PZT nanowire from sol-gel method. Under both tensile and bending effect, the peak voltage of the nanogenerator was 1.6V and the output power could reach 0.03 μW when the load resistance was 6MΩ [83].Later, K. J. Lee et al developed generators via Au-$BaTiO_3$-Pt structure thin films on a polydimethylsiloxane (PDMS) substrate. The tensile and compressive stress from bending effects produced current up to 26 nA, output voltage up to 1.0V and

power density up to 7 mW/cm^3 [82]. Also, film-type and island-type nanocapacitors are fabricated via W. Lee et al to develop potential applications of nanosized oxide capacitors for resistive memory (ReRAM) devices [80]. P. K. Purohit and M. C. Mcalpine et al prepared buckled PZT ribbons and the waves geometry could increases maximum tensile strain without fracture. The piezoelectric effect could be up to 70% and the current could be up to 60 pA [79]. Another piezoelectric ZnO thin film systems with plastic substrates were prepared via Y. S. Kim et al. Direct depositing and printing method made films low-cost and easy for large area production. The film structures exhibits a high elasticity and resistance to mechanical fatigue. The output voltage could reach 0.8V and output current density could reach 100 nA/cm^2 [78].

Among these researches, few of them provide a comprehensive study to compare the influence of geometry shape and size scale. In Chapter 4, the experiments have verified simulation results on the mechanical indentation response of PSZT nanoislands and thin films. The objectives of this part are: (i) to obtain a comprehensive understanding of the nanoindentation response of several nanostructures of relaxor ferroelectric materials with different size scales; and (ii) to identify optimum combination of geometry shape and size scale when contact between piezoelectric materials and rigid tips were applied to design piezoelectric devices for energy harvesting.

Different from the parts in characterization of piezoelectric materials via nanoindentation, materials properties (elastic modulus, piezoelectric coefficient and dielectric coefficient) are all the same but geometry structures are varied. Here, one kind of relaxor ferroelectric materials, PMN-0.33PT (Table 5), is chosen as the materials for energy harvesting. Three kinds of nanostructures, including nanoislands (hemispherical), nanowire (single line with height/width=1 and double

line height/width=2) and thin film, with very thin layer of platinum and silicon substrate (20 μm). The size range of these structures is from 200 nm to 1000 nm as shown in Figure 17 and a conducting spherical tip with 10 μm radius is used to generate electric charges. To avoid cracks propagation in materials, the indentation depth is limited to 15% of the piezoelectric structure's length along loading direction. Three dimensional finite element models are built with around 30,000 8-node linear piezoelectric brick (C3D8E) elements and 300,000 8-node linear brick, reduced integration (C3D8R) elements. To ensure the accurate when calculating electric charges, at least 50 elements are in contact with indenter at the maximum displacement. The force-depth and charge-depth curves are both recorded to analyze the final results.

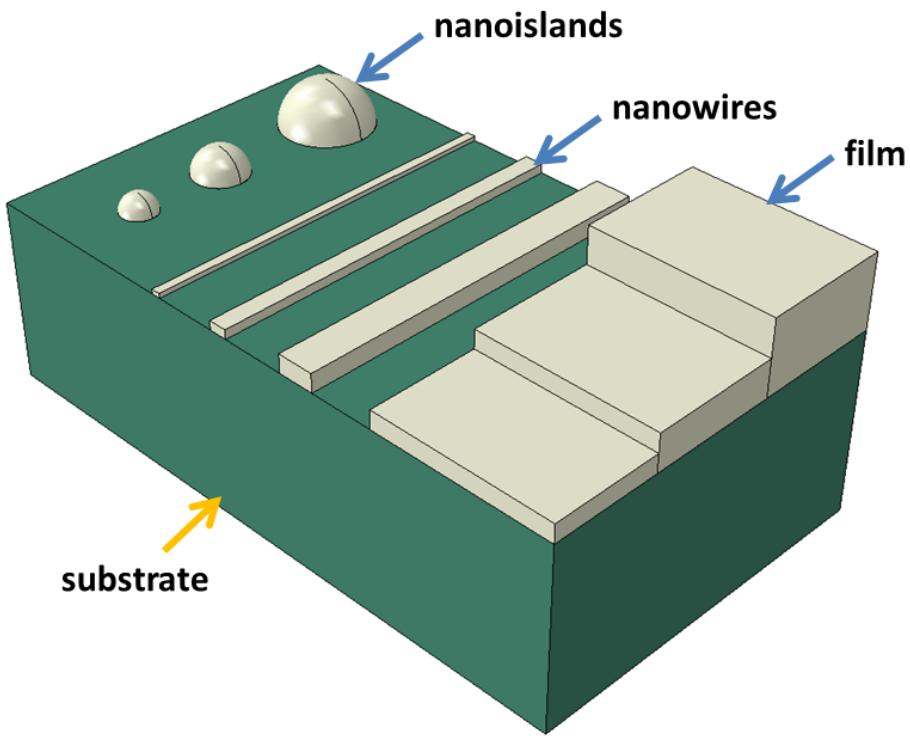

Figure 17 Schematic illustrating the indentation of piezoelectric nanostructures: nanoislands (hemispherical), nanowire (single structure with cross section height/width=1 and double structure with cross section height/width=2) and thin film

5.2 Results and discussion

1. From the view of nanostructures on same size scale, nanoislands require minimum load to indent and thin films require maximum to indent. The reason for this trend is accused for contact regions with a specific tip: nanoislands always provided the minimum contact area and thin film provided the maximum. With increase of the size, the load from nanoislands is close to the nanowire at 1000 nm.(Figure 18)
2. From the charge-depth curves of all 200 nm nanostructures, different from trends in force-depth curves, nanowire (double) could generate most charge and nanoislands generate least. Thin film could offer more charge than nanowire (single) but smaller than nanowire (double). This trend is also presented in 500 nm and 1000 nm nanostructures. In nanowires, the piezoelectric structures are bended via spherical indenter and substrate so there are extra charges generated. Meanwhile, contact area can also affect total number of charges collected via indenter. So here, the position of nanowire (double) and thin films are switched. (Figure 19)

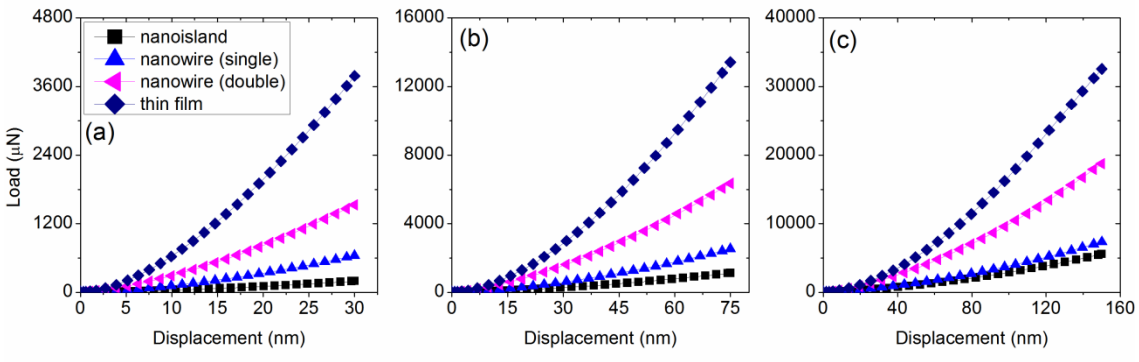

Figure 18 The force-depth response obtained from conducting indentations on piezoelectric nanostructures nanoislands, nanowire (single), nanowire (double) and thin film with silicon substrate on same size scale (a) 200nm (b) 500nm and (c) 1000nm

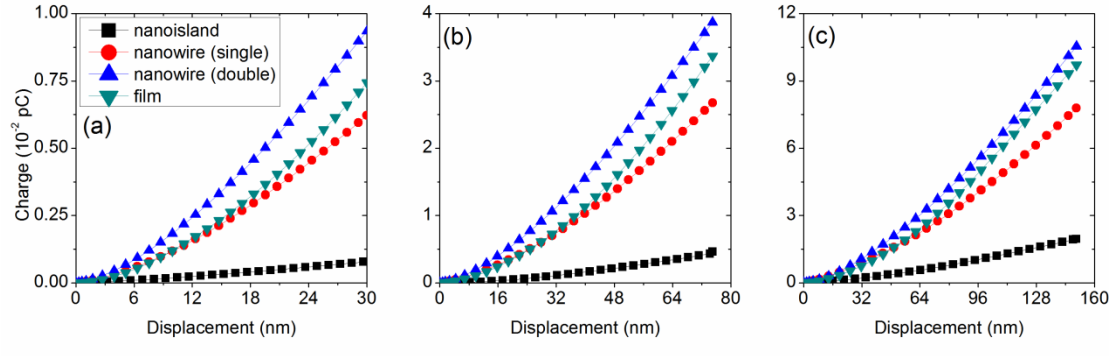

Figure 19 The charge-depth response obtained from conducting indentations on piezoelectric nanostructures nanoislands, nanowire (single), nanowire (double) and thin film with silicon substrate on same size scale (a) 200nm (b) 500nm and (c) 1000nm

3. From the view of geometry size, in nanoislands and nanowires, the larger structures are stiffer than smaller structures and provide more charges while in thin films, the smaller structures are stiffer than larger structures and provide more charges. This trend could be also illustrated via the change in contact regions. At same indentation depth, the contact region increases with the size increasing for nanoislands and nanowires, however, in thin film, since the indenter is always fully contacted with materials, this effect could be ignored since the contact region is affected by geometry shape very little. The difference in thickness brought in substrate effects during the contact: the elastic modulus of Si (185 Gpa) substrate is much higher than the normal elastic component of PMN-0.33PT (C_{33}=115 Gpa). So with a stiffer substrate, the thinner films display stiffer mechanical response than thicker films. Meanwhile, with higher stress concentration, more charges are collected. (Figure 20 and Figure 21)

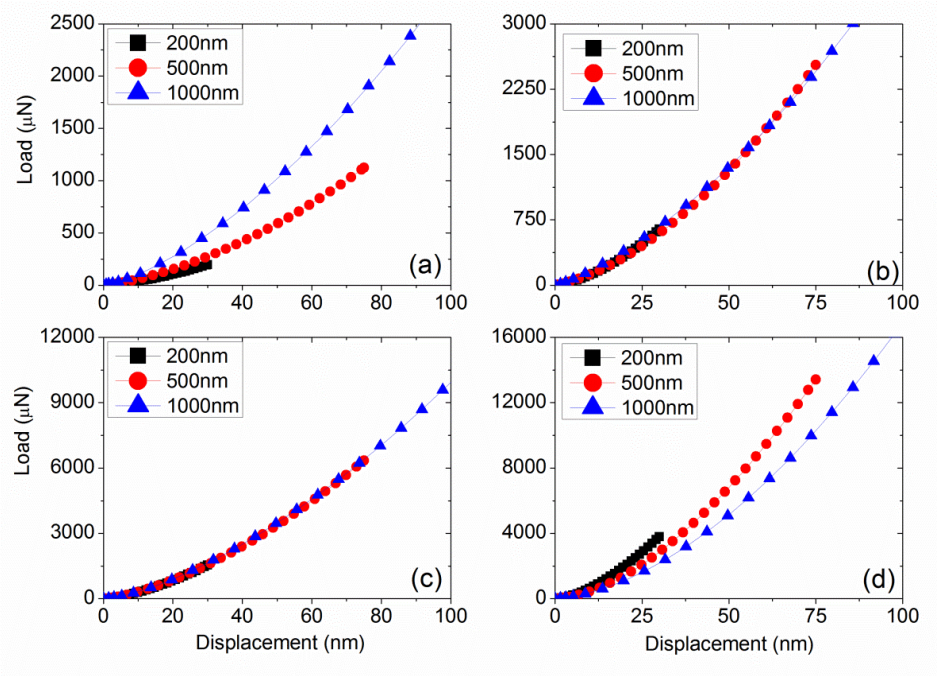

Figure 20 The force-depth response obtained from conducting indentations on piezoelectric nanostructures on different size scale, 200nm, 500nm and 1000nm with silicon substrate on same size scale (a) nanoislands, (b) nanowire (single), (c) nanowire (double) and (d) thin film

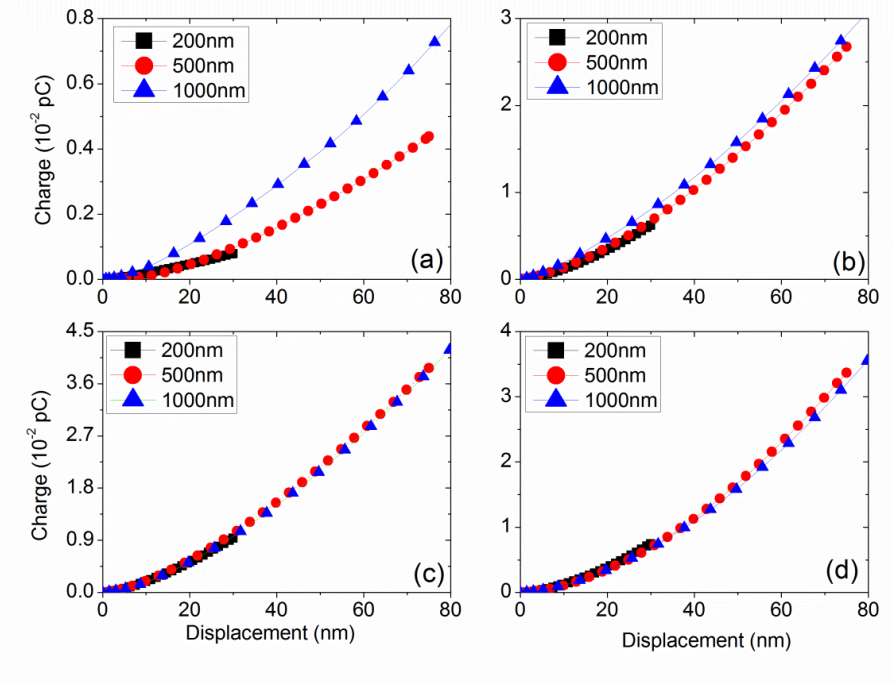

Figure 21 The charge-depth response obtained from conducting indentations on piezoelectric nanostructures on different size scale, 200nm, 500nm and 1000nm with silicon substrate on same size scale (a) nanoislands, (b) nanowire (single), (c) nanowire (double)

4. To illustrate the geometry influence on the charge collecting, the relationship between the width of the thin nanowire and total number of reaction charges are investigated. The height of the nanowire is assumed as 500nm and the width increases from 500nm (single nanowire) to 5000nm (thin film). From Figure 22, initially, the number of charges increased with the width increasing. Although the geometry shape restricts volume of piezoelectric materials in contact, the bending effects could bring in extra charges. With the increase of width, the restriction of geometry shape gradually becomes weakened but the bending effect still works. So the value reaches the peak when the ratio of width/height is round 3. Later, the bending effect gradually disappears until the indenter tip fully touches with piezoelectric materials when nanowire could provide same contact area as thin films. So after the peak, the number of charges decreases. The value becomes same as the value from thin films when the ratio of width/height is round 5. (Figure 22)
5. Compared between the load-ratio (for example, the maximum load of 500nm nanoislands/ the maximum load of 200nm nanoislands = 5.755) and size-ratio (for example, 500nm/200nm=2.5), it is recognizing that the nanoislands increase more than three other structures with the increase of size. Meanwhile, thin films could provide the maximum load on same sizes scale, but get minimum rate of increase on the load with same size ratio raise in current research. In the relationship between charge-ratio (for example, the maximum load of 500nm thin nanoislands/ the maximum load of 200nm thin film = 4.53) and size-ratio (for example, 500nm/200nm=2.5), it is also found that the charge generated from nanoislands increase more than three other structures with the increase of size. Then, nanowire (double) could provide the most charges on the same sizes scale, but get minimum rate of increase on the charge with

same size ratio raise. (Figure 19 and Figure 23)

6. To illustrate the substrate effect in thin films, the silicon carbide, of which elastic modulus could reach 430 Gpa, is chosen as a stiffer substrate [96]. The charge-depth and force-depth curves are exhibited in Figure 24. The substrate influences the contact response initially so there is not significant inflection in the curves as shown in Chapter 4. Also, the bifurcation appeared since the indenter contacted with film. Then silicon carbide substrate renders the thin film stiffer and provides more charge than silicon substrate with same indentation depth. However, the stress concentration on the interface between piezoelectric materials and silicon carbide is significantly higher than interface of piezoelectric materials and silicon.

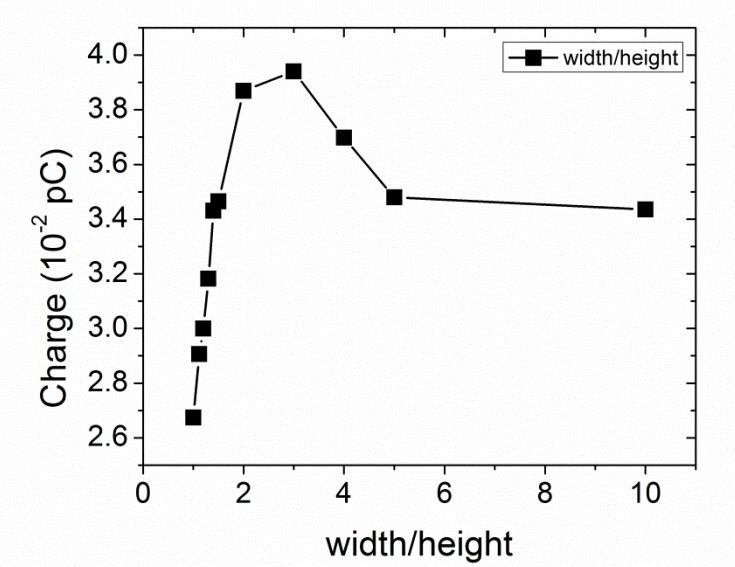

Figure 22 The relationship between maximum charges obtained from conducting indentations and geometry factor, width/height, for nanowire with silicon substrate

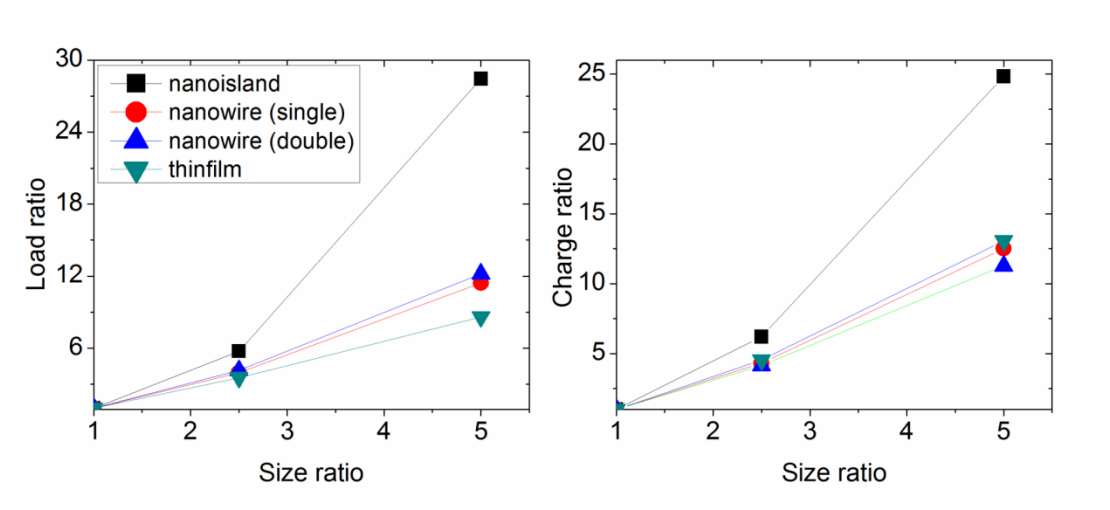

Figure 23 The relationship between load/charge obtained from conducting indentations ratios with size ratios for all the nanostructures with silicon substrate, for example, the maximum load of 500nm nanoislands/ the maximum load of 200nm nanoislands, the size ratio was 2.5 and load ratio was 5.755

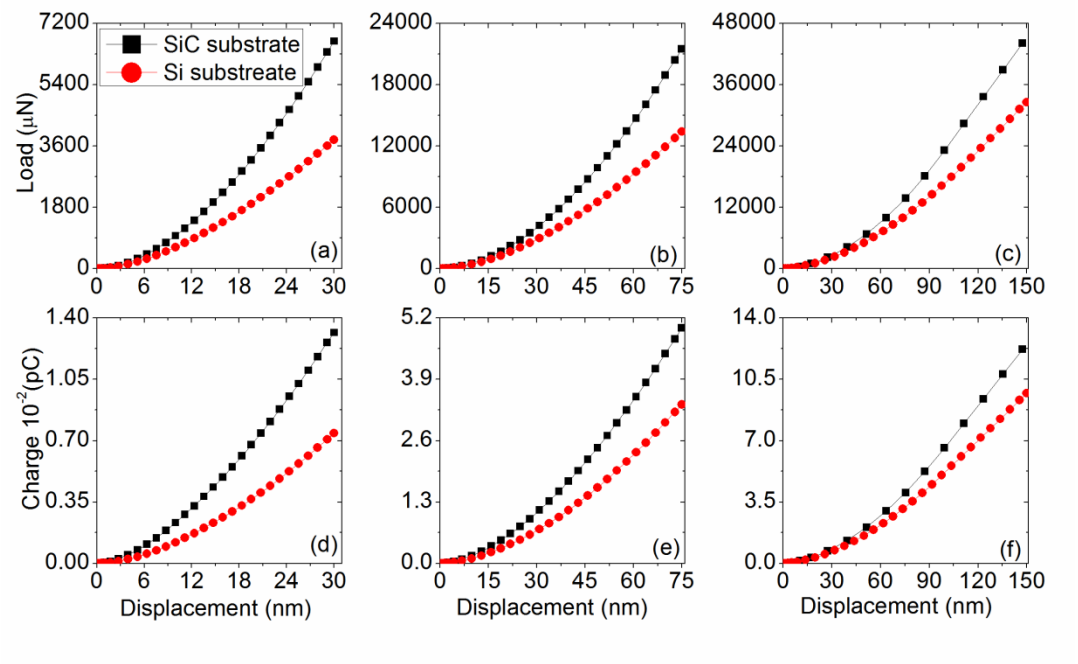

Figure 24 The force-depth and charge-depth response obtained from conducting spherical indentations on piezoelectric thin films with silicon and silicon carbide substrate: (a) force-depth of 200nm thin film (d) charge-depth of 200nm thin film (b) force-depth of 500nm thin film (e) charge-depth of 500nm thin film (c) force-depth of 1000nm thin film (f) charge-depth of 1000nm thin film

7. Although the indenter was not fully contacted with piezoelectric materials, the force-depth and charge-depth curves could fit the power law relationship for spherical indenter. (Table 8)

Table 8 Fitting data of force/charge-depth curves from conducting indentation response of nanostructures via power law P=Ch1.5 (the unit of C =μN/(nm)1.5) and Q= Cqh1.5 (the unit of Cq=10-2pC/(nm)1.5)

	size		nanoislands	nanowire single	nanowire double	thin film
Force vs. Depth	200nm	C	1.16862	3.81471	9.25331	22.49749
		error	0.00293	0.01536	0.00994	0.12538
		error/C	0.002507	0.004027	0.001074	0.005573
	500nm	C	1.69675	3.80254	9.65975	19.89796
		error	0.00389	0.01518	0.01716	0.16886
		error/C	0.002293	0.003992	0.001776	0.008486
	1000nm	C	2.9562	3.90589	10.06092	17.33242
		error	0.01005	0.01398	0.02131	0.1396
		error/C	0.0034	0.003579	0.002118	0.008054
	size		nanoislands	nanowire single	nanowire double	thin film
Charge vs. Depth	200nm	C_q	0.000497	0.00378	0.00575	0.00437
		error	4E-06	1.99E-06	9.3E-06	3.11E-05
		error/C_q	0.008049	0.000527	0.001618	0.00712
	500nm	C_q	0.000659	0.00411	0.00603	0.00495
		error	3.68E-06	2.9E-06	1.28E-05	5.06E-05
		error/C_q	0.005589	0.000706	0.002124	0.010231
	1000nm	C_q	0.00108	0.00426	0.00579	0.00525
		error	2.48E-06	1.17E-05	9.05E-06	3.23E-05
		error/C_q	0.002293	0.002751	0.001562	0.006145

5.3 Conclusions

According to the results above, the finite element method gives a comprehensive study on the influence of nanostructures on the indentation responses: the nanowires with proper geometry shape can provide maximum electric charges than thin film and nanoislands; larger scale of nanoislands and nanowire are stiffer but larger scale of thin film is softer; nanoislands would offer more ratio of charge with the same increase on the size scale. Also the substrate effects on mechanic and electric indentation response of thin film are presented. These results will be great helpful to design and fabrication of energy harvesting device.

Chapter 6 Nanoindentation of piezoelectric materials: Part V — Understanding the effects of electric fields: implication for

6.1 Introduction

Electrical fields have been applied to understand the ultrahigh strain/strength of relaxor ferroelectric materials [1, 2, 74]. Moreover, other effects from electrical fields, such as fracture toughness, bending test and polarization switching, have been reported [60, 97-100]. However, in most of previous research focusing nanoindentation responses of piezoelectric materials, the electric field was only applied paralleled to the polarization direction of piezoelectric materials. This prevented comprehensive understandings on influence of piezoelectric materials from electric field during nanoindentation test.

So based on previous research as well as current research results, two important questions in the field remain to be fully answered:

1. From a fundamental science perspective, is the nanoindentation response of piezoelectric materials influenced by external electric fields?
2. From a technological perspective, can the influence of the electric fields on the indentation response of piezoelectric materials be better understood to impact the growing field of piezo force microscopy?

Hence, the objectives of the this chapter are: (i) to obtain a comprehensive understanding of the nanoindentation response of several classes of anisotropic

piezoelectric materials under the influence of external electric fields; and (ii) to identify conditions where electric fields can be used in conjunction with nanoindentation to characterize the domain structure of piezoelectric materials.

In this chapter, Nine classes of indentations are identified depending on the poling direction of the material with respect to the indentation direction (i.e., longitudinal or transverse) and the direction of the electric field which could be aligned parallel to the poling direction or orthogonal to the poling direction (Figure 25). A similar three-dimensional finite element model was used as previous chapter. Four model piezoelectric materials – Barium Sodium niobate [51], Relaxor Ferroelectric [70], Barium Sodium Niobate [53], and Lithium Niobate [54] that, respectively, exhibit 4mm, 4mm, mm2, and 3m crystal symmetry are used as substrate materials for the indentation study. The indenter is modeled as being elastically rigid, and electrically insulating or conducting. Yet, too high electrical field can lead depolarization or dielectric breakdown in piezoelectric materials.

Considering the maximum electrical field for hard PZT is 2400V/mm [101], in current research, ±1KV/mm and ±2KV/mm are amounted on piezoelectric materials to clarify the effect of electrical field during the indentation process. It is supposed that under this electric field, the piezoelectric materials just went through elastic expansion or compression and no dielectric breakdown or poled direction switching happened.

6.2 Results and suggestion for piezo-force microscopy

From the indentation study of nine classes of piezoelectric materials, the following principal observations are made:

1. In indentations of Classes I and II, where the material is longitudinally poled

and the electrical field is applied in a direction that is orthogonal to the poling direction, the mechanical indentation stiffness and the electrical indentation stiffness are not influenced by the electric fields. (Figure 26**)**

2. In indentations of Class III, where the material is longitudinally poled and the electric field is applied in a direction that is parallel to the poling direction, the mechanical and electrical indentation stiffnesses are significantly influenced by the magnitude and direction of the applied electric field. Amongst the four piezoelectric materials considered in the present study, Barium Titanate and Relaxor Ferroelectric which have relatively higher piezoelectric constant e_{33}, exhibit greater sensitivities to the applied electric fields. A positive electric field tends to make the indented material mechanically and electrically stiffer while a negative electric field has the opposite effect. This electric field effect on the mechanical indentation stiffness is conceptually similar to the influence of a residual stress in (a non-piezoelectric) indented material on the mechanical indentation stiffness where a compressive residual stress results in a greater resistance to indentation while a tensile residual stress provides less resistance to indentation as compared to indentations on a stress-free material. (Figure 27**)**
3. In indentations of Classes IV and VIII, where the material is poled transverse to the direction of indentation and the electric field is applied along the poling direction, there is a significant influence of the electric field on the mechanical indentation response of the materials with a positive electric field resulting in a more compliant indentation response while a negative electric field resulting in a more stiffer indentation response. A positive electric field stretches the piezoelectric material in a direction that is perpendicular to the direction of

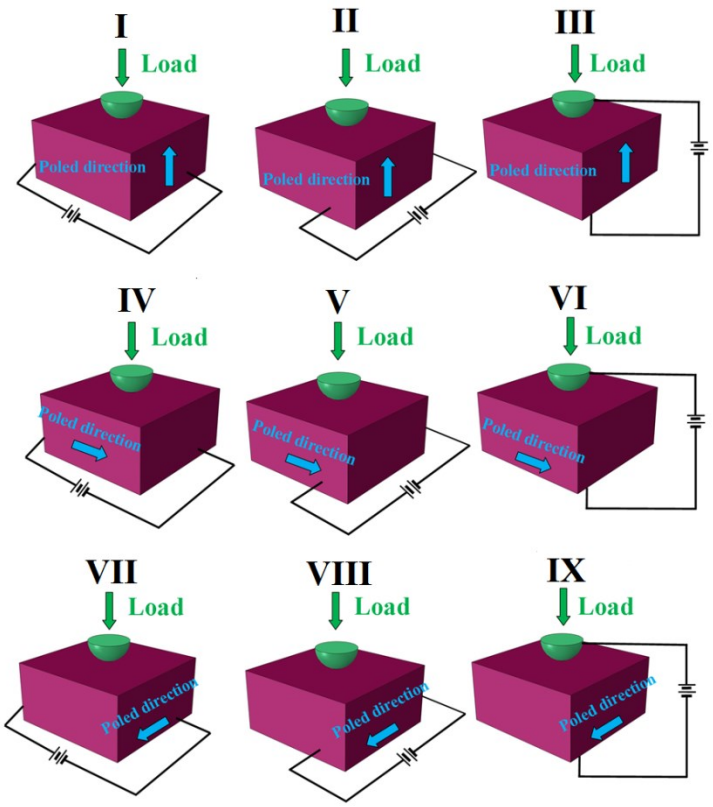

Figure 25 Schematic illustrating nine classes of indentations to capture the influence of electric fields on the effective indentation response of anisotropic piezoelectric materials with conical, indenters.

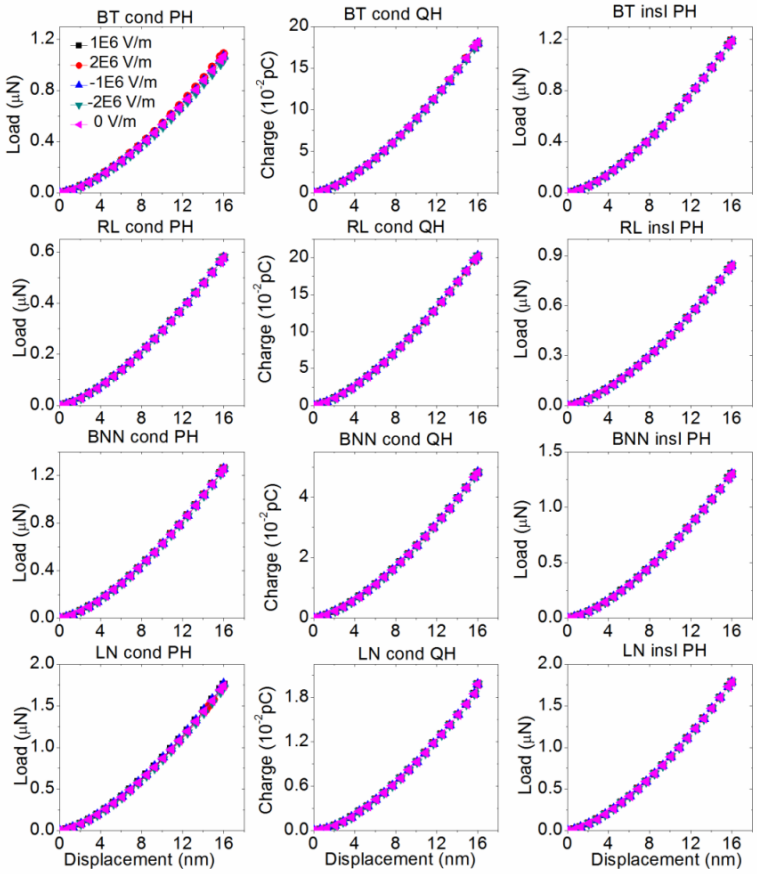

Figure 26 The force-depth and the charge-depth indentation response obtained from indentations of Classes I and III for four model piezoelectric materials – Barium Titanate (BT), Relaxor Ferroelectric (RL), Barium Sodium Niobate and Lithium Niobate. (The radius of the spherical indenter is 10μm.)

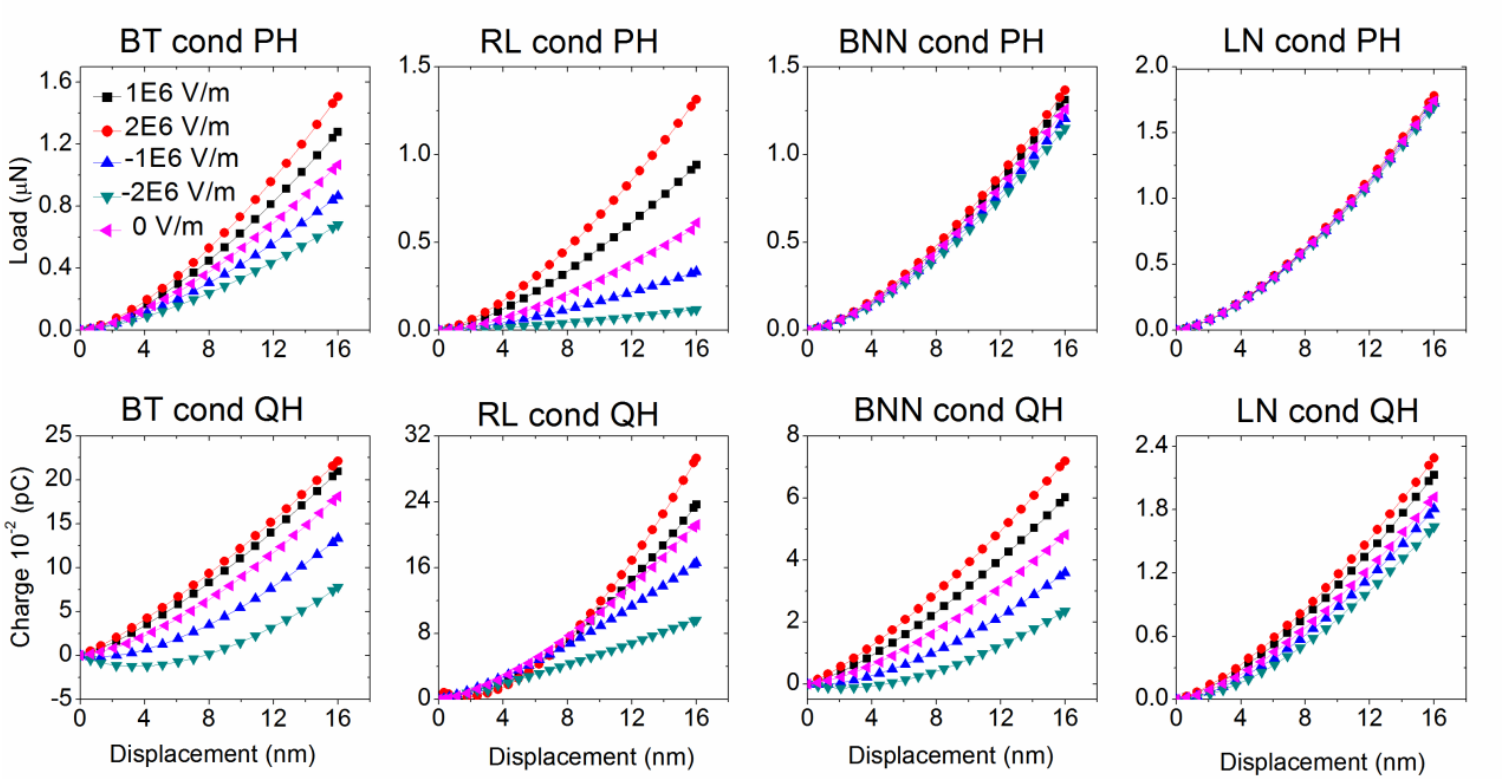

Figure 27 The force-depth and the charge-depth indentation response obtained from indentations of Classes II for four model piezoelectric materials – Barium Titanate (BT), Relaxor Ferroelectric (RL), Barium Sodium Niobate (BSN) and Lithium Niobate (LN). (The radius of the spherical indenter is 10μm.)

indentation, thus making the mechanical indentation response of the material to be more compliant. (Figure 28**)**

4. In indentations of Classes VI and IX, where the material is transversely poled and the electric field is applied along the indentation direction, the electrical indentation stiffness is influenced moderately by the applied electric fields, while the mechanical indentation stiffness remains relatively unchanged. (Figure 29**)**
5. In indentations of Classes V and VII, where the material is transversely poled and the applied electric field is neither aligned with the poling direction nor the indentation direction, the electrical indentation stiffness is influenced slightly by the applied electric fields, while the mechanical indentation stiffness remains relatively unchanged. (Figure 30**)**
6. From a technological perspective, existing piezo force microscopy methods use out-of-plane electric fields to identify piezoelectrically active domains in the out-of-plane direction. The present study demonstrates that in-plane electric fields can be used to identify domains which are poled along specific in-plane directions. (Figure 31**)**
7. Generally, materials with weak piezoelectric ability (BNN & LN) show less variance than those with strong piezoelectric ability (BT&RL) under same electric fields. Also considering more complex properties of lithium niobate (e_{22}), on some cases, some charges could still be detected under Class IV-IX.
8. In Class II, analytical models could present the force-depth and charge depth relationships for Barium Titanate. However, the results did not match well with current finite element models and the problems would come from ignoring the coupling electric field, which is dominated by both external electrical field and local electric field from piezoelectric effect. (Figure 32)

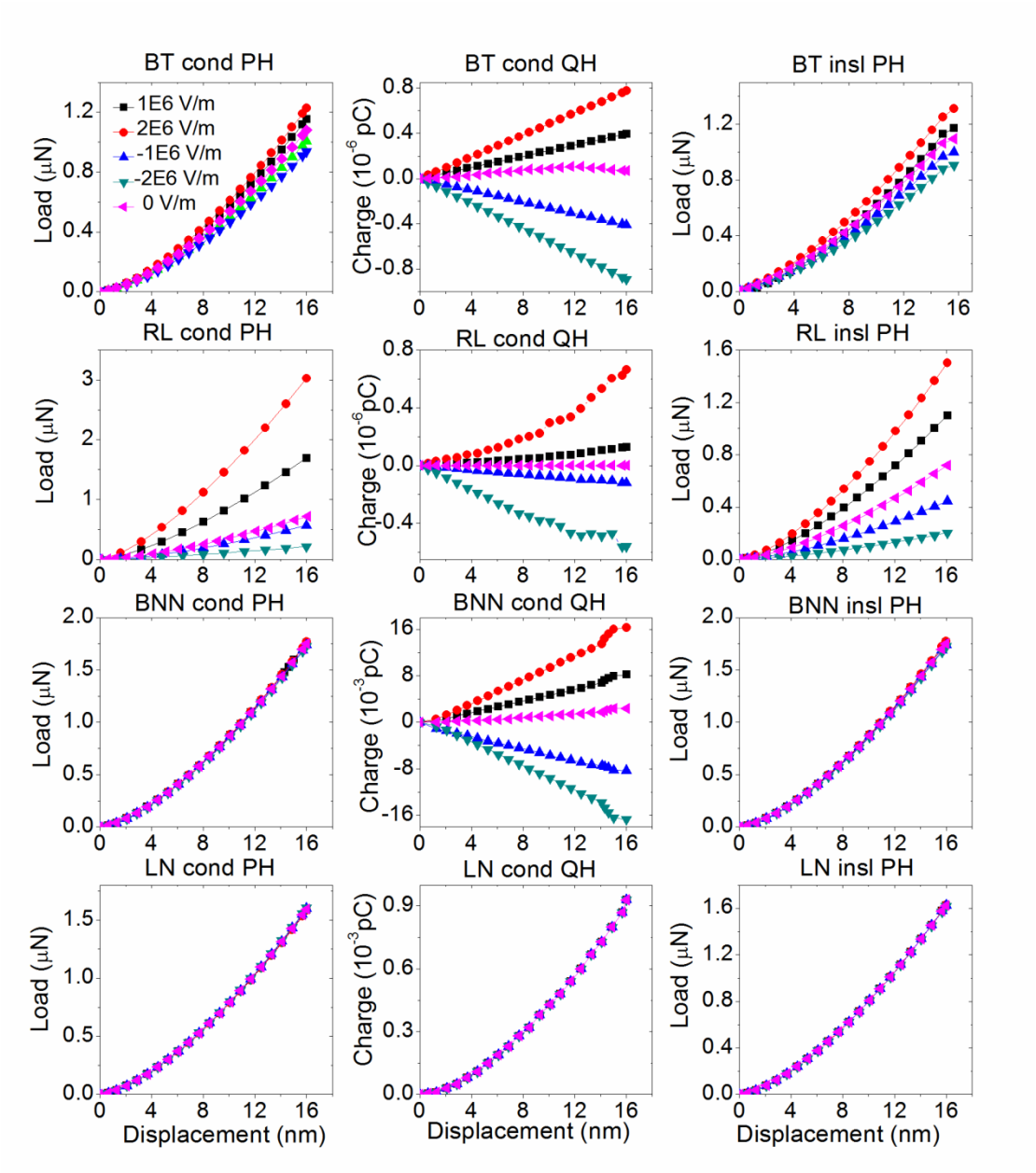

Figure 28 The force-depth and the charge-depth indentation response obtained from indentations of Classes IV and VIII for four model piezoelectric materials –Barium Titanate (BT), Relaxor Ferroelectric (RL), Barium Sodium Niobate (BSN) and Lithium Niobate (LN). (The radius of the spherical indenter is 10μm.)

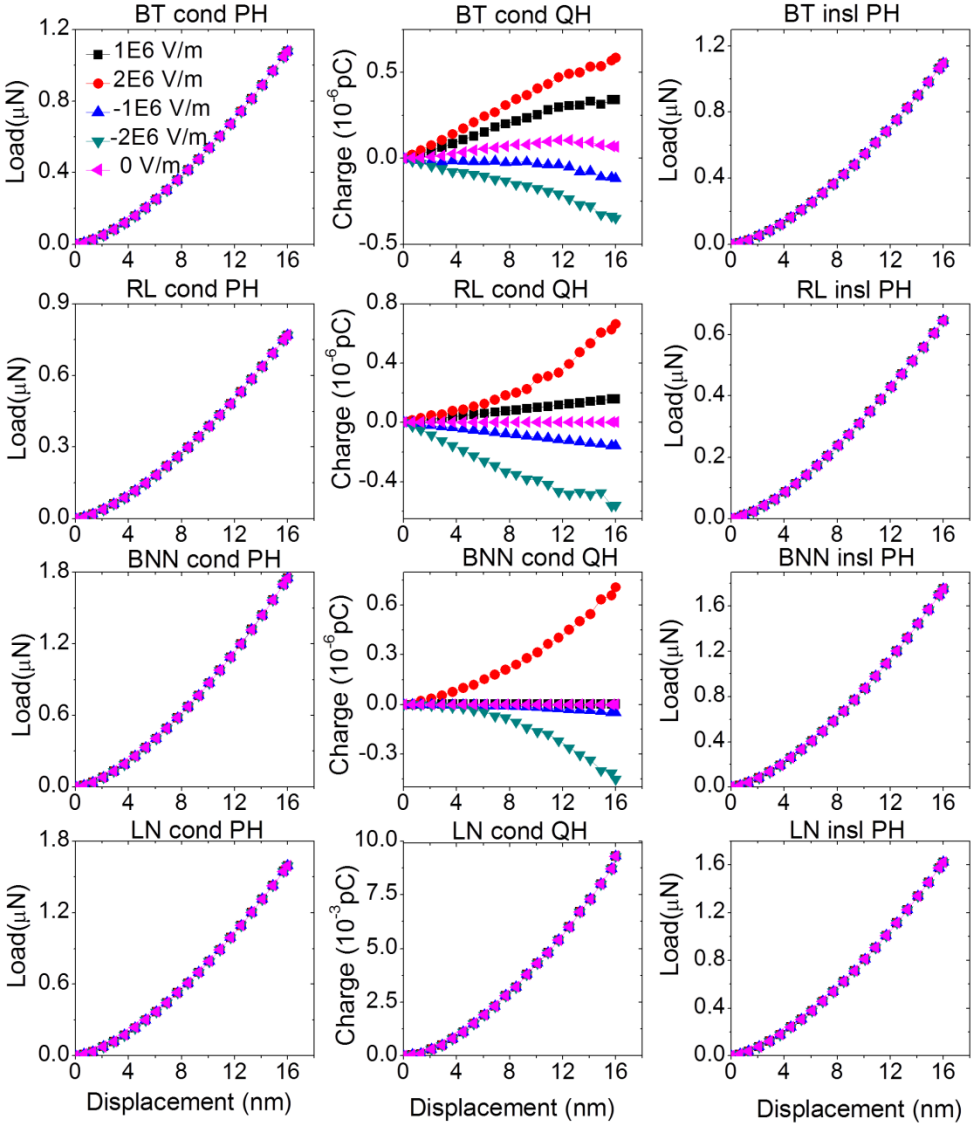

Figure 29 The force-depth and the charge-depth indentation response obtained from indentations of Classes V and VII for four model piezoelectric materials –Barium Titanate (BT), Relaxor Ferroelectric (RL), Barium Sodium Niobate (BSN) and Lithium Niobate (LN). (The radius of the spherical indenter is 10μm.)

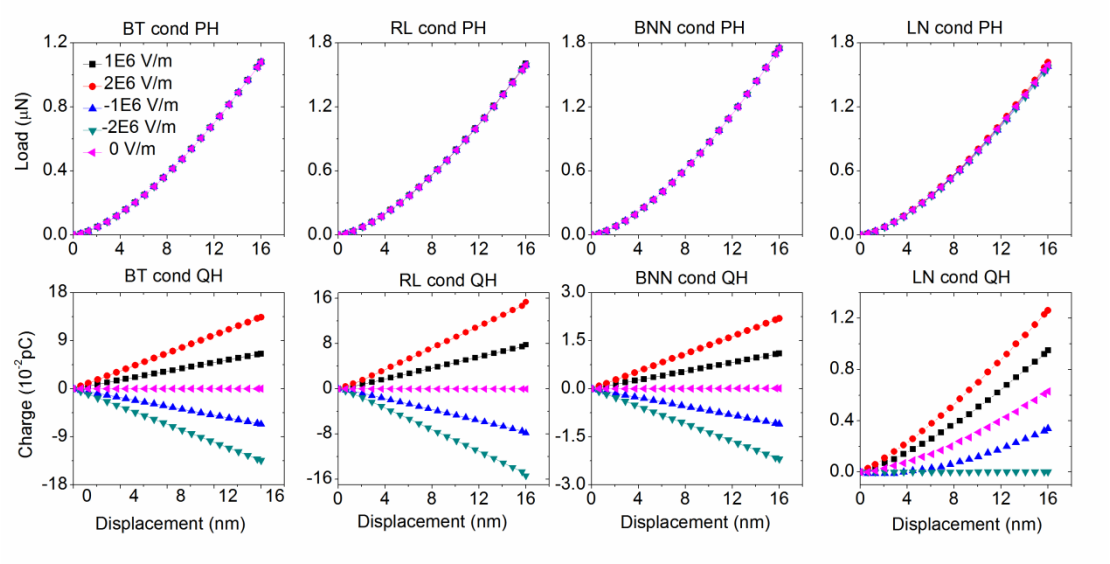

Figure 30 The force-depth and the charge-depth indentation response obtained from indentations of Classes VI and IX for four model piezoelectric materials –Barium Titanate (BT), Relaxor Ferroelectric (RL), Barium Sodium Niobate (BSN) and Lithium Niobate (LN). (The radius of the spherical indenter is 10μm.)

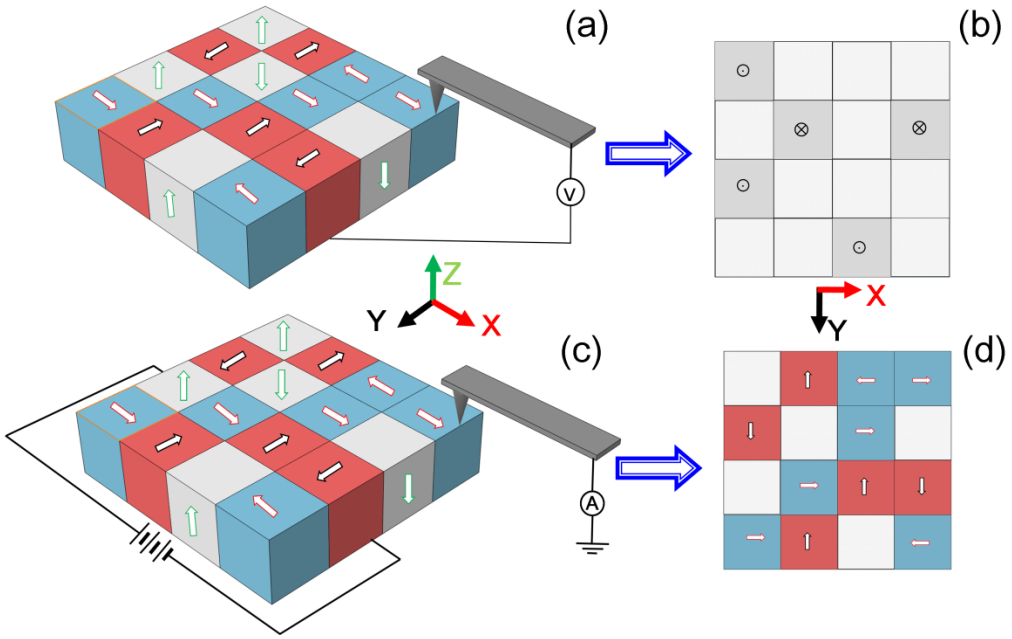

Figure 31 (a, b) Typical piezo force microscopy techniques allow the identification and characterization of the domains of a piezoelectric material that are active along the out-of-plane (z) direction by applying an electric field in the out-of-plane (z) direction. (c, d) The approach presented in this study allows for the characterization of the domains that are active along the in-plane (e.g., x) direction by applying an electric field along the in-plane (x) direction.

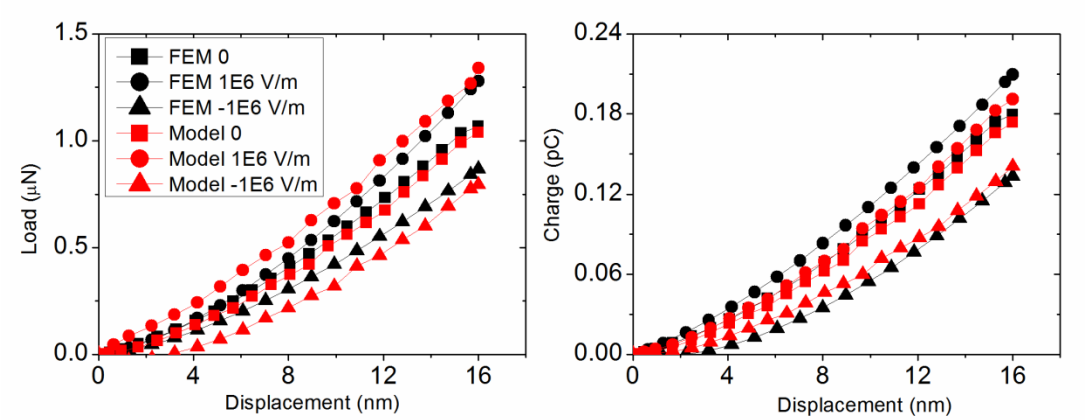

Figure 32 The force-depth and charge-depth indentation response obtained from the finite element analysis with the analytical model predictions [27] for the transversely isotropic Lead Zirconate Titanate system for spherical indentation using a conducting indenter

6.3 Conclusions

Overall, in this part, a three-dimensional finite element model has been developed to accurately capture the effect of external electric fields on the indentation response of piezoelectric materials. Nine classes of indentations are carefully examined and it is demonstrated that the indentation response of piezoelectric materials is, in general, strongly influenced by electric fields when the electric field is aligned parallel to the poling direction. In particular, the present study demonstrates that in-plane electric fields can be used in conjunction with nanoindentation to identify domains which are poled along specific in-plane directions, thus enhancing the versatility of the piezo force microcopy technique for characterizing active materials.

Chapter 7 Conclusions

With new developed three-dimensional finite element simulation models has been applied to collect micro/nanoindentation responses on anisotropic piezoelectric materials with multi-geometry shapes, including bulk, films, nanoislands and nanowire. From large number of simulations and related data, following conclusions could be highlighted:

1. The force/charge-depth curves of anisotropic piezoelectric materials (Lithium niobate, Barium sodium niobate and Relaxor ferroelectric materials etc.) could fit power law.
2. The dominant factors (C_{33} and e_{33}) for mechanical/electrical indentation response of bulk materials are confirmed.
3. Simulation results could be verified by corresponding experiments as well as analytical models.
4. Piezoelectric effect renders bulk materials stiffer and piezoelectric nanostructures with higher piezoelectric coefficient (etc. e_{33} or d_{33}) could have better electromechanical performance.
5. Elastic modulus of substrate could influence the indentation response at the initial of indentation however the elastoplastic of substrate could influence the response after a certain indentation depth.
6. Nanowire with bending effect could offer more charges than thin films under spherical indentation.
7. The polarization direction of piezoelectric materials can be determined via analysis nanoindentation responses under appropriate electric boundary conditions.

Chapter 8 Suggestions and future works

8.1 Forward and reverse analysis

As presented in literature survey, by dimensional analysis, materials' properties could be extracted from indentation results with proper algorithm and analysis. However, such method has been few used for piezoelectric materials. With the finite element models in current research, the forward analysis, which means the indentation response could be calculated from materials properties, has been finished. For transversely isotropic piezoelectric material, as dominant factors presented in Chapter 3, the materials will be simplified as: elastic modulus (C_{33} and C_{13}), piezoelectric coefficient (e_{31} and e_{15}) and dielectric coefficient (ε). Then, more than three hundreds materials combinations will be listed and the electric and mechanics responses under indentation will be calculated by FEM. Then dimensionless functions are derived by fitting polynomial functions based on the dimensional analysis. Furthermore, an algorithm is needed to deduce materials' properties from these responses and this is reverse analysis. Meanwhile, to verify this process, uniqueness and sensitivity analysis should be considered.

8.2 Further FE simulation

In current research, the bulk materials are set as single crystal materials with same properties. Later, piezoelectric composites, such as 0-3, 1-3 and 2-2 types will be considered [102-104]. Also porous piezoelectric materials, with various

pores geometric shapes and porosities, will be designed and the indentation behavior will be simulated.

Another aspect would be potential application in biology, such as bones, joints and teeth. Bones could be treated as porous piezoelectric composites and nanoindentation tests could help people in test the electromechanical performance of artificial bone and joints [105-107].

Also, as piezoelectric materials widely applied in energy harvesting devices, it will be helpful if we could predict electric current, efficient, fatigue and fractures from finite element simulations. Considering the default element model for piezoelectric materials in current commercial package is only available for elastic deformation and not sufficient to accomplish these new goals. New constitutive equations and element models with nano effects and plasticity should be derived and subroutines code for dynamic elements will be required in future.

8.3 Experimental verification

Since some indentation experiments had been done on transverse isotropic piezoelectric materials, indentation experiments on relaxor ferroelectric materials and other anisotropic piezoelectric materials (lithium niobate and barium sodium niobate) will be prepared. Also as we discovered in Chapter 6, nanoindentation will helpful to determine the in-plane direction of polarization piezoelectric materials. So it will be interesting to design and prepare such experiments on small size of piezoelectric materials.

Chapter 9 Thesis outcomes

9.1 Publications

- Cheng G, Venkatesh TA. Nanoindentation response of anisotropic piezoelectric materials. Phil Mag Lett. 2012;92(6):278-87.
- Cheng G, Venkatesh TA. Dominant factors influencing the nanoindentation response of piezoelectric materials: a case study in relaxor ferroelectrics. Phil Mag Lett. 2013;93(2):116-128.
- Cheng G, Venkatesh TA. The influence of electrical field and electrical potential on nanoindentation of anisotropic piezoelectric materials (submitted)
- Nili H, Cheng G, Venkatesh TA, Sriram S, Bhaskaran M. Correlation between nanomechanical and piezoelectric properties of thin films: An experimental and finite element study. Mater Lett. 2013;90:148-51.
- Cheng G, Venkatesh TA. Nanoindentation response of piezoelectric nanoislands: experiments and simulations (to be submitted in May 2013)
- Cheng G, Venkatesh TA. Nanoindentation response of nanostructures: the influence of geometry and size scale.(to be submitted in June 2013)

9.2 Patents

- **Cheng, G**. and Venkatesh, T. A. (2011) “Method to Determine the Poling State and Poling Direction of Anisotropic Piezoelectric Materials through Instrumented Indentation”, Patent Disclosure.
- **Cheng, G**. and Venkatesh, T. A. (2013) “Method to Determine the In-plane Piezoelectric Characteristics of Thin Film Materials through Nanoindentation under Electric Fields”, Patent Disclosure

References

[1] Tichy J. Fundamentals of piezoelectric sensorics : mechanical, dielectric, and thermodynamical properties of piezoelectric materials. New York: Springer, 2010.

[2] Heywang W. Piezoelectricity. New York: Springer, 2008.

[3] Cady WG. Piezoelectricity; an introduction to the theory and applications of electromechanical phenomena in crystals. New York, London,: McGraw-Hill Book Company, inc., 1946.

[4] Xu F, Chu F, Trolier-McKinstry S. Longitudinal piezoelectric coefficient measurement for bulk ceramics and thin films using pneumatic pressure rig. J Appl Phys 1999;86:588.

[5] Lefki K, Dormans GJM. Measurement of Piezoelectric Coefficients of Ferroelectric Thin-Films. J Appl Phys 1994;76:1764.

[6] Park GT, Choi JJ, Ryu J, Fan HQ, Kim HE. Measurement of piezoelectric coefficients of lead zirconate titanate thin films by strain-monitoring pneumatic loading method. Appl Phys Lett 2002;80:4606.

[7] Saha R, Xue ZY, Huang Y, Nix WD. Indentation of a soft metal film on a hard substrate: strain gradient hardening effects. J Mech Phys Solids 2001;49:1997.

[8] Chen X, Vlassak JJ. Numerical study on the measurement of thin film mechanical properties by means of nanoindentation. J Mater Res 2001;16:2974.

[9] Oliver WC, Pharr GM. Nanoindentation in materials research: Past, present, and future. Mrs Bull 2010;35:897.

[10] Oliver WC, Pharr GM. Measurement of hardness and elastic modulus by instrumented indentation: Advances in understanding and refinements to methodology. J Mater Res 2004;19:3.

[11] Oliver WC, Pharr GM. An Improved Technique for Determining Hardness

and Elastic-Modulus Using Load and Displacement Sensing Indentation Experiments. J Mater Res 1992;7:1564.

[12] Tian M, Venkatesh TA. Indentation of shape memory polymers: Characterization of thermomechanical and shape recovery properties. Polymer 2013;54:1405.

[13] Fischer-Cripps AC. Introduction to contact mechanics. New York: Springer, 2007.

[14] Lan HZ, Venkatesh TA. On the sensitivity characteristics in the determination of the elastic and plastic properties of materials through multiple indentation. J Mater Res 2007;22:1043.

[15] Lan HZ, Venkatesh TA. Determination of the elastic and plastic properties of materials through instrumented indentation with reduced sensitivity. Acta Mater 2007;55:2025.

[16] Lan H, Venkatesh TA. On the uniqueness and sensitivity issues in determining the elastic and plastic properties of power-law hardening materials through sharp and spherical indentation. Philos Mag 2007;87:4671.

[17] Dao M, Chollacoop N, Van Vliet KJ, Venkatesh TA, Suresh S. Computational modeling of the forward and reverse problems in instrumented sharp indentation. Acta Mater 2001;49:3899.

[18] Venkatesh TA, Van Vliet KJ, Giannakopoulos AE, Suresh S. Determination of elasto-plastic properties by instrumented sharp indentation: Guidelines for property extraction. Scripta Mater 2000;42:833.

[19] Cheng YT, Cheng CM. Scaling, dimensional analysis, and indentation measurements. Mat Sci Eng R 2004;44:91.

[20] Melkumyan SA, Ulitko AF. Axisymmetric Contact Problem of Electroelasticity for a Half-Space. Sov Appl Mech+ 1987;23:836.

[21] Fan H, Sze KY, Yang W. Two-dimensional contact on a piezoelectric half-space. Int J Solids Struct 1996;33:1305.

[22] Giannakopoulos AE. Strength analysis of spherical indentation of piezoelectric materials. J Appl Mech-T Asme 2000;67:409.

[23] Sridhar S, Giannakopoulos AE, Suresh S, Ramamurty U. Electrical response during indentation of piezoelectric materials: A new method for material characterization. J Appl Phys 1999;85:380.

[24] Giannakopoulos AE, Suresh S. Theory of indentation of piezoelectric materials. Acta Mater 1999;47:2153.

[25] Yang FQ. Analysis of the axisymmetric indentation of a semi-infinite piezoelectric material: The evaluation of the contact stiffness and the effective piezoelectric constant. J Appl Phys 2008;103.

[26] Yang FQ. Electromechanical interaction of linear piezoelectric materials with a surface electrode. J Mater Sci 2004;39:2811.

[27] Liu M, Yang F. Three-dimensional finite element simulation of the Berkovich indentation of a transversely isotropic piezoelectric material: effect of material orientation. Model Simul Mater Sc 2013;21:045014.

[28] Liu M, Yang F. Orientation effect on the Boussinesq indentation of a transversely isotropic piezoelectric material. Int J Solids Struct 2013;50:2542.

[29] Wang JH, Chen CQ, Lu TJ. Indentation responses of piezoelectric films. J Mech Phys Solids 2008;56:3331.

[30] Karapetian E, Kachanov M, Kalinin SV. Nanoelectromechanics of piezoelectric indentation and applications to scanning probe microscopies of ferroelectric materials. Philos Mag 2005;85:1017.

[31] Karapetian E, Kachanov M, Sevostianov I. The principle of correspondence between elastic and piezoelectric problems. Arch Appl Mech 2002;72:564.

[32] Makagon A, Kachanov M, Kalinin SV, Karapetian E. Indentation of spherical and conical punches into piezoelectric half-space with frictional sliding: Applications to scanning probe microscopy. Phys Rev B 2007;76.

[33] Kamble SN, Kubair DV, Ramamurty U. Indentation strength of a piezoelectric ceramic: Experiments and simulations. J Mater Res 2009;24:926.

[34] Chen WQ, Pan EN, Wang HM, Zhang CZ. Theory of indentation on multiferroic composite materials. J Mech Phys Solids 2010;58:1524.

[35] Sridhar S, Giannakopoulos AE, Suresh S. Mechanical and electrical responses of piezoelectric solids to conical indentation. J Appl Phys 2000;87:8451.

[36] Ramamurty U, Sridhar S, Giannakopoulos AE, Suresh S. An experimental study of spherical indentation on piezoelectric materials. Acta Mater 1999;47:2417.

[37] Rar A, Pharr GM, Oliver WC, Karapetian E, Kalinin SV. Piezoelectric nanoindentation. J Mater Res 2006;21:552.

[38] Wong MF, Zeng K. Deformation behavior of PZN-6%PT single crystal during nanoindentation. Philos Mag 2008;88:3105.

[39] Bahr DF, Robach JS, Wright JS, Francis LF, Gerberich WW. Mechanical deformation of PZT thin films for MEMS applications. Mat Sci Eng a-Struct 1999;259:126.

[40] Koval V, Reece MJ, Bushby AJ. Ferroelectric/ferroelastic behavior and piezoelectric response of lead zirconate titanate thin films under nanoindentation. J Appl Phys 2005;97.

[41] Chima-Okereke C, Bushby AJ, Reece MJ, Whatmore RW, Zhang Q. Experimental, analytical, and finite element analyses of nanoindentation of multilayer PZT/Pt/SiO2 thin film systems on silicon wafers. J Mater Res 2006;21:409.

[42] Fang TH, Chang WJ, Lin CM. Nanoindentation characterization of ZnO thin films. Mat Sci Eng a-Struct 2007;452:715.

[43] Song ST, Zheng XJ, Zheng H, Liu W. Evaluation of engineering/piezoelectric

constants of piezoelectric thin film by combining nanoindentation test with FEM. Comp Mater Sci 2012;63:134.

[44] Wu YF, Yu HY, Chen WQ. Indentation responses of piezoelectric layered half-space. Smart Materials and Structures 2013;22.

[45] Ding HJ, Chenbuo, Liangjian. General solutions for coupled equations for piezoelectric media. Int J Solids Struct 1996;33:2283.

[46] Chen WQ. On piezoelastic contact problem for a smooth punch. Int J Solids Struct 2000;37:2331.

[47] Lu HY, Cheng SY, Ho NJ. Micro-Indentation-Induced Domain Switching in Tetragonal Barium Titanate. J Am Ceram Soc 2008;91:3721.

[48] Liu D, Chelf M, White KW. Indentation plasticity of barium titanate single crystals: Dislocation influence on ferroelectric domain walls. Acta Mater 2006;54:4525.

[49] Zheng XJ, Zhou YC, Li JY. Nano-indentation fracture test of Pb(Zr(0.52)Ti(0.48))O(3) ferroelectric thin films. Acta Mater 2003;51:3985.

[50] Zheng XJ, Zhou YC, Liu JM, Li AD. Interfacial adhesion analysis of Pb(Zr(0.52)Ti(0.48))O(3) (PZT) thin films by nano-indentation test. Phys Lett A 2002;304:110.

[51] Jaffe H, Berlinco.Da. Piezoelectric Transducer Materials. Pr Inst Electr Elect 1965;53:1372.

[52] Zhang R, Jiang B, Cao WW. Elastic, piezoelectric, and dielectric properties of multidomain 0.67Pb(Mg1/3Nb2/3)O-3-0.33PbTiO(3) single crystals. J Appl Phys 2001;90:3471.

[53] Warner AW, Coquin GA, Fink JL. Elastic and Piezoelectric Constants of Ba2nanb5o15. J Appl Phys 1969;40:4353.

[54] Warner AW, Onoe M, Coquin GA. Determination of Elastic and Piezoelectric Constants for Crystals in Class (3m). J Acoust Soc Am 1967;42:1223.

[55] Liu XZ, Zhang SJ, Luo J, Shrout TR, Cao WW. A complete set of material properties of single domain 0.26Pb(In(1/2)Nb(1/2))O(3)-0.46Pb(Mg(1/3)Nb(2/3))O(3)-0.28PbTiO(3) single crystals. Appl Phys Lett 2010;96.

[56] Li F, Zhang SJ, Xu Z, Wei XY, Luo J, Shrout TR. Electromechanical properties of tetragonal Pb(In(1/2)Nb(1/2))O(3)-Pb(Mg(1/3)Nb(2/3))O(3)-PbTiO(3) ferroelectric crystals. J Appl Phys 2010;107.

[57] Liu XZ, Zhang SJ, Luo J, Shrout TR, Cao WW. Complete set of material constants of Pb(In(1/2)Nb(1/2))O(3)-Pb(Mg(1/3)Nb(2/3))O(3)-PbTiO(3) single crystal with morphotropic phase boundary composition. J Appl Phys 2009;106.

[58] Zhou D, Wang FF, Luo LH, Chen J, Ge WW, Zhao XY, Luo HS. Characterization of complete electromechanical constants of rhombohedral 0.72Pb(Mg(1/3)Nb(2/3))-0.28PbTiO(3) single crystals. J Phys D Appl Phys 2008;41.

[59] Shukla R, Rajan KK, Gandhi P, Lim LC. Complete sets of elastic, dielectric, and piezoelectric properties of [001]-poled Pb(Zn1/3Nb2/3)O-3-(6-7)%PbTiO3 single crystals of [110]-length cut. Appl Phys Lett 2008;92.

[60] Xu GY, Zhong Z, Bing Y, Ye ZG, Shirane G. Electric-field-induced redistribution of polar nano-regions in a relaxor ferroelectric. Nat Mater 2006;5:134.

[61] He CJ, Zhou D, Wang FF, Xu HQ, Lin D, Luo HS. Elastic, piezoelectric, and dielectric properties of tetragonal Pb(Mg1/3Nb2/3)O-3-PbTiO3 single crystals. J Appl Phys 2006;100.

[62] Peng J, Luo HS, He TH, Xu HQ, Lin D. Elastic, dielectric, and piezoelectric characterization of 0.70Pb(Mg1/3Nb2/3)O-3-0.30PbTiO(3) single crystals. Mater Lett 2005;59:640.

[63] McLaughlin EA, Liu TQ, Lynch CS. Relaxor ferroelectric PMN-32%PT crystals under stress, electric field and temperature loading: II-33-mode measurements. Acta

Mater 2005;53:4001.

[64] Zhou DY, Kamlah M, Munz D. Uniaxial compressive stress dependence of the high-field dielectric and piezoelectric performance of soft PZT piezoceramics. J Mater Res 2004;19:834.

[65] Zhang SJ, Randall CA, Shrout TR. Dielectric, piezoelectric and elastic properties of tetragonal BiScO3-PbTiO3 single crystal with single domain. Solid State Commun 2004;131:41.

[66] McLaughlin EA, Liu TQ, Lynch CS. Relaxor ferroelectric PMN-32%PT crystals under stress and electric field loading: I-32 mode measurements. Acta Mater 2004;52:3849.

[67] Cao H, Schmidt VH, Zhang R, Cao WW, Luo HS. Elastic, piezoelectric, and dielectric properties of 0.58Pb(Mg1/3Nb2/3)O-3-0.42PbTiO(3) single crystal. J Appl Phys 2004;96:549.

[68] Jiang WH, Zhang R, Jiang B, Cao WW. Characterization of piezoelectric materials with large piezoelectric and electromechanical coupling coefficients. Ultrasonics 2003;41:55.

[69] Cao H, Fang BJ, Xu HQ, Luo HS. Elastic, dielectric, piezoelectric and electromechanical properties of tetragonal Pb(Mg1/3Nb2/3)O-3-PbTiO3 (PMN-PT). J Inorg Mater 2003;18:465.

[70] Zhang R, Jiang W, Jiang B, Cao W. Elastic, Dielectric and Piezoelctric Coefficients of Domain Engineered 0.70Pb(Mg1/3Nb2/3)O3-0.30PbTiO3 Single Crystal. Fundamental Physics of Ferroelectrics 2002, vol. 626: American Institute of Physics Conference Proceeding, 2002. p.188.

[71] Zhang R, Jiang B, Jiang WH, Cao WW. Anisotropy in domain engineered 0-92Pb(Zn(1/3)Nb(2/3))O(3)-0.08PbTiO(3) single crystal and analysis of its property fluctuations. Ieee T Ultrason Ferr 2002;49:1622.

[72] Cao H, Luo HS. Elastic, piezoelectric and dielectric properties of Pb(Mg1/3Nb2/3)O-3-38%PbTiO3 single crystal. Ferroelectrics 2002;274:309.

[73] Yin JH, Jiang B, Cao WW. Elastic, piezoelectric, and dielectric properties of 0.955Pb(Zn1/3Nb2/3) O-3-0.45PbTiO(3) single crystal with designed multidomains. Ieee T Ultrason Ferr 2000;47:285.

[74] Park SE, Shrout TR. Ultrahigh strain and piezoelectric behavior in relaxor based ferroelectric single crystals. J Appl Phys 1997;82:1804.

[75] Shang JK, Tan X. Indentation-induced domain switching in Pb(Mg1/3Nb2/3)O-3-PbTiO3 crystal. Acta Mater 2001;49:2993.

[76] Zhang R, Jiang B, Cao WW, Amin A. Complete set of material constants of 0.93Pb(Zn1/3Nb2/3)O-3-0.07PbTiO(3) domain engineered single crystal. J Mater Sci Lett 2002;21:1877.

[77] Wu WW, Bai S, Yuan MM, Qin Y, Wang ZL, Jing T. Lead Zirconate Titanate Nanowire Textile Nanogenerator for Wearable Energy-Harvesting and Self-Powered Devices. Acs Nano 2012;6:6231.

[78] Chung SY, Kim S, Lee JH, Kim K, Kim SW, Kang CY, Yoon SJ, Kim YS. All-Solution-Processed Flexible Thin Film Piezoelectric Nanogenerator. Adv Mater 2012;24:6022.

[79] Qi Y, Kim J, Nguyen TD, Lisko B, Purohit PK, McAlpine MC. Enhanced Piezoelectricity and Stretchability in Energy Harvesting Devices Fabricated from Buckled PZT Ribbons. Nano Lett 2011;11:1331.

[80] Han H, Kim Y, Alexe M, Hesse D, Lee W. Nanostructured Ferroelectrics: Fabrication and Structure-Property Relations. Adv Mater 2011;23:4599.

[81] Xu S, Qin Y, Xu C, Wei YG, Yang RS, Wang ZL. Self-powered nanowire devices. Nat Nanotechnol 2010;5:366.

[82] Park KI, Xu S, Liu Y, Hwang GT, Kang SJL, Wang ZL, Lee KJ. Piezoelectric

BaTiO3 Thin Film Nanogenerator on Plastic Substrates. Nano Lett 2010;10:4939.

[83] Chen X, Xu SY, Yao N, Shi Y. 1.6 V Nanogenerator for Mechanical Energy Harvesting Using PZT Nanofibers. Nano Lett 2010;10:2133.

[84] Liao Y, Sodano HA. Structural Effects and Energy Conversion Efficiency of Power Harvesting. J Intel Mat Syst Str 2009;20:505.

[85] Qin Y, Wang XD, Wang ZL. Microfibre-nanowire hybrid structure for energy scavenging. Nature 2008;451:809.

[86] Su WS, Chen YF, Hsiao CL, Tu LW. Generation of electricity in GaN nanorods induced by piezoelectric effect. Appl Phys Lett 2007;90.

[87] Gao PX, Song JH, Liu J, Wang ZL. Nanowire piezoelectric nanogenerators on plastic substrates as flexible power sources for nanodevices. Adv Mater 2007;19:67.

[88] Anton SR, Sodano HA. A review of power harvesting using piezoelectric materials (2003-2006). Smart Mater Struct 2007;16:R1.

[89] Sriram S, Bhaskaran M, Ahluwalia R, Nguyen TG, Ng N, Srolovitz DJ, Kalantar-Zadeh K, Mitchell A. Surface Morphology Induced Localized Electric Field and Piezoresponse Enhancement in Nanostructured Thin Films. Acs Nano 2011;5:1067.

[90] Bhaskaran M, Sriram S, Ruffell S, Mitchell A. Nanoscale Characterization of Energy Generation from Piezoelectric Thin Films. Adv Funct Mater 2011;21:2251.

[91] Sriram S, Bhaskaran M, Mitchell DRG, Short KT, Holland AS, Mitchell A. Microstructural and Compositional Analysis of Strontium-Doped Lead Zirconate Titanate Thin Films on Gold-Coated Silicon Substrates. Microsc Microanal 2009;15:30.

[92] Sriram S, Bhaskaran M, Mitchell A, Mitchell DRG, Kostovski G. Nanocolumnar Preferentially Oriented PSZT Thin Films Deposited on Thermally Grown Silicon Dioxide. Nanoscale Res Lett 2009;4:29.

[93] Sriram S, Bhaskaran M, Holland AS, Short KT, Latella BA. Measurement of high piezoelectric response of strontium-doped lead zirconate titanate thin films using a

nanoindenter. J Appl Phys 2007;101.

[94] Glazounov AE, Kungl H, Reszat JT, Hoffmann MJ, Kolleck A, Schneider GA, Wroblewski T. Contribution from ferroelastic domain switching detected using X-ray diffraction to R-Curves in lead zirconate titanate ceramics. J Am Ceram Soc 2001;84:2921.

[95] Jonnalagadda KN, Chasiotis I, Yagnamurthy S, Lambros J, Pulskamp J, Polcawich R, Dubey M. Experimental Investigation of Strain Rate Dependence of Nanocrystalline Pt Films. Exp Mech 2010;50:25.

[96] Wolfenden A, Burris CP, Singh M. Young's modulus and vibrational damping of sintered silicon carbide ceramics at high temperatures. J Mater Sci Lett 1999;18:1995.

[97] Singh J, Soni NC, Lamba GS. Dielectric properties of piezoelectric transducer materials measured at high electric field. Indian J Pure Ap Phy 1996;34:162.

[98] Schneider GA, Heyer V. Influence of the electric field on Vickers indentation crack growth in BaTiO3. J Eur Ceram Soc 1999;19:1299.

[99] Zhang TY. Effects of static electric field on the fracture behavior of piezoelectric ceramics. Acta Mech Sinica 2002;18:537.

[100] Kumar S, Singh RN. Crack propagation in piezoelectric materials under combined mechanical and electrical loadings. Acta Mater 1996;44:173.

[101] Branwood A, Hurd JD, Tredgold RH. Dielectric Breakdown in Barium Titanate. Brit J Appl Phys 1962;13:528.

[102] Iyer S, Venkatesh TA. Electromechanical response of porous piezoelectric materials: Effects of porosity connectivity. Appl Phys Lett 2010;97.

[103] Marcheselli C, Venkatesh TA. Electromechanical response of 1-3 piezoelectric composites with hollow fibers. Appl Phys Lett 2008;93.

[104] Kar-Gupta R, Venkatesh TA. Electromechanical response of piezoelectric composites: Effects of geometric connectivity and grain size. Acta Mater 2008;56:3810.

[105] Panagiotopoulou O. Finite element analysis (FEA): Applying an engineering method to functional morphology in anthropology and human biology. Ann Hum Biol 2009;36:609.

[106] Zhang J, Niebur GL, Ovaert TC. Mechanical property determination of bone through nano- and micro-indentation testing and finite element simulation. J Biomech 2008;41:267.

[107] Wu JZ, Herzog W, Epstein M. Evaluation of the finite element software ABAQUS for biomechanical modelling of biphasic tissues. J Biomech 1998;31:165.